**Project Report
ATC-164**
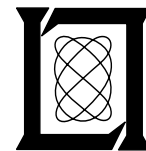
The Effectiveness of Adaptive PRF Selection in Minimizing Range Obscuration in the TDWR System

S. C. Crocker

27 July 1989

Lincoln Laboratory

MASSACHUSETTS INSTITUTE OF TECHNOLOGY

LEXINGTON, MASSACHUSETTS

1. Report No. DOT/FAA/PS-88-18	2. Government Accession No.	3. Recipient's Catalog No.
4. Title and Subtitle The Effectiveness of Adaptive PRF Selection in Minimizing Range Obscuration in the TDWR System		5. Report Date 27 July 1989
		6. Performing Organization Code
7. Author(s) Sandra C. Crocker		8. Performing Organization Report No. ATC-164
9. Performing Organization Name and Address Lincoln Laboratory, MIT P.O. Box 73 Lexington, MA 02173-0073		10. Work Unit No. (TRAIS)
		11. Contract or Grant No. DTFA-01-L-83-4-10579
12. Sponsoring Agency Name and Address Department of Transportation Federal Aviation Administration Program Engineering Service Washington, DC 20591		13. Type of Report and Period Covered Project Report
		14. Sponsoring Agency Code

15. Supplementary Notes

16. Abstract

An adaptive procedure for selecting radar pulse repetition frequency (PRF) has been developed as the primary means of minimizing the occurrence of range aliased echoes within operationally significant coverage areas (e.g., airport runways) of the Terminal Doppler Weather Radar (TDWR) system. This procedure underwent extensive testing at the S-Band TDWR testbed while located in Denver, CO, where it was judged to be highly successful at preserving the integrity of data collected within the vicinity of the Stapleton International Airport runways.

The actual TDWR system will operate at a C-Band frequency, and an increase in potential range obscuration is expected over that experienced by the S-Band testbed. This report discusses the anticipated performance of the PRF selection procedure in the C-Band environment by extrapolating results obtained using S-Band testbed data. The results conclusively demonstrate the efficacy of adaptive PRF selection as a method by which to reduce potential range obscuration. A worst-case scenario, for example, indicates that over 20% of the TDWR radar data collected about the airport runways has the potential for being contaminated with range aliased echoes at any given time during TDWR surveillance operations. With adaptive PRF selection, however, the expected obscuration is reduced to only 3%. (The corresponding figures for the S-Band testbed are shown to be 14% rather than 20% and 1% rather than 3%). While adaptive PRF selection can substantially reduce range obscuration, it cannot totally eliminate the problem. An enhancement to the PRF selection strategy, which further reduces the potential range obscuration, is introduced and recommended. Additionally, the complementary use of pulse-to-pulse phase modulation to exact valid velocity measurements in the presence of range contamination is discussed and preliminary experimental results presented.

17. Key Words		18. Distribution Statement

radar pulse repetition
  frequency
Terminal Doppler Weather
  Radar (TDWR)
	range aliased echoes
	Doppler weather radar
	radar phase coding
	range ambiguities
		Document is available to the public through the National Technical Information Service, Springfield, VA 22161.

19. Security Classif. (of this report) Unclassified	20. Security Classif. (of this page) Unclassified	21. No. of Pages 53	22. Price

FORM DOT F 1700.7 (8-72) Reproduction of completed page authorized

ABSTRACT

An adaptive procedure for selecting radar pulse repetition frequency (PRF) has been developed as the primary means of minimizing the occurrence of range aliased echoes within operationally significant coverage areas (e.g., airport runways) of the Terminal Doppler Weather Radar (TDWR) system. This procedure underwent extensive testing at the S–Band TDWR testbed while located in Denver, CO, where it was judged to be highly successful at preserving the integrity of data collected within the vicinity of the Stapleton International Airport runways.

The actual TDWR system will operate at a C–Band frequency, and an increase in potential range obscuration is expected over that experienced by the S–Band testbed. This report discusses the anticipated performance of the PRF selection procedure in the C–Band environment by extrapolating results obtained using S–Band testbed data. The results conclusively demonstrate the efficacy of adaptive PRF selection as a method by which to reduce potential range obscuration. A worst–case scenario, for example, indicates that over 20% of the TDWR radar data collected about the airport runways has the potential for being contaminated with range aliased echoes at any given time during TDWR surveillance operations. With adaptive PRF selection, however, the expected obscuration is reduced to only 3%. (The corresponding figures for the S–Band testbed are shown to be 14% rather than 20% and 1% rather than 3%.) While adaptive PRF selection can substantially reduce range obscuration, it cannot totally eliminate the problem. An enhancement to the PRF selection strategy which further reduces the potential range obscuration is introduced and recommended. Additionally, the complementary use of pulse–to–pulse phase modulation to extract valid velocity measurements in the presence of range contamination is discussed and preliminary experimental results presented.

TABLE OF CONTENTS

LIST OF ILLUSTRATIONS

LIST OF TABLES

1.0 Introduction

The Federal Aviation Administration is developing the TDWR system as a fully automated means of identifying and issuing warnings for meteorological wind shear hazards (e.g., microbursts and gust fronts) within the immediate vicinity of high traffic airports. These warnings will be conveyed to aircraft pilots in order that potentially hazardous takeoffs or landings be averted.

In a pulsed Doppler weather radar, one of the most serious causes of data quality degradation is attributed to range aliased echoes from distant storms [1]. This range contamination can occur in the immediate vicinity of a meteorological hazard, possibly obscure the event, and thus decrease the probability of detecting it. In other instances, range contaminated data can present a radar signature similar to that of a wind shear hazard, and perhaps cause an algorithm to issue a false alarm. In order for the TDWR system to achieve a high probability of detecting meteorological hazards, while maintaining a low probability of false alarms, an effective means of dealing with range contamination is required. This report addresses the performance of the principal mechanism to be used by the TDWR system; i.e., data adaptive PRF control.

1.1 Review of Fundamental Equations

Two fundamental equations define limitations for the unambiguous measurement of range and radial velocity in a Doppler radar that is pulsed at a constant interpulse period [1,2]. These equations are provided below as (1) and (2) where R and V represent the unambiguous range and the unambiguous velocity interval, respectively, T_p the interpulse period, and λ the wavelength of the radar.

$$R = (\ c\ T_p\ )\ /\ 2 \quad \text{, where } c \text{ is the speed of light.} \tag{1}$$

$$V = (+/-)\ \lambda\ /\ 4\ T_p \text{ , where + and - indicate velocity away from and toward the} \tag{2}$$
$$\text{radar, respectively.}$$

Several observations regarding the relationship of various parameters within these two equations prove relevant to the problem at hand. First, as seen in (1) and (2), T_p is directly related to R yet inversely related to V. This implies that, by decreasing the interpulse period, one simultaneously decreases the unambiguous range interval and increases the unambiguous velocity interval. Second, as noted in (2), a direct relationship exists between radar wavelength and V. Shortening λ (by increasing the operating frequency), while holding the other parameter constant, inherently decreases the interval over which velocity may be measured unambiguously.

1.2 Statement of Problem

A TDWR testbed facility, configured and operated by MIT Lincoln Laboratory [3], has collected radar measurement data and exercised meteorological identification algorithms [4,5] in support of the TDWR development effort over the past several years in a variety of geographical locations, most recently in Denver, CO. This testbed facility is comprised of a pencil-beam radar that radiates at 2865 MHz, with λ equal to approximately 10 cm. In order to ensure reasonable Nyquist intervals for the measurement of radial velocities associated with typical weather phenomena, this S-Band radar operates at PRFs   from

700 to 1220 Hz (T_p = 1 / PRF). The bounds of the unambiguous range intervals associated with this span of PRF values are easily calculated (1) as 214 and 123 km, respectively. Assuming that distant storms as far away as 425 km may be detected by the radar, this span of PRF values could result in range folded obscuration from 2nd, 3rd, and possibly even 4th trip distant weather echoes, depending on PRF and storm location.

The actual TDWR system will radiate at approximately 5650 MHz with a beamwidth of 0.5 deg [6]. The TDWR λ is roughly 5 cm which by (2) implies an inherent reduction in the ability to unambiguously measure a storm's radial velocity. To compensate for this reduction at the C-Band frequency, a higher set of PRF values will be required over those currently used at the testbed. By (1), a higher set of PRFs further implies reduced unambiguous range intervals. PRF values as high as 2000 Hz are anticipated, which will result in unambiguous range intervals as short as 75 km. This means that obscuration from 2nd, 3rd, 4th, and possibly even 5th and 6th trip distant weather echoes may be experienced in the TDWR environment; providing an effective means for dealing with this obscuration presents a significant challenge.

1.3 Overview of Report

Quantifying range obscuration and assessing the effectiveness of techniques designed to minimize this obscuration in the S-Band testbed and the C-Band TDWR environments is the subject of this report. Section 2.0 describes the analysis methods used throughout this investigation and introduces a data set (from the testbed distant weather database) that serves as the object data set for this report. Section 3.0 quantifies the potential range obscuration that may be experienced in the S-Band and C-Band environments, and provides a measure of the effectiveness of the primary technique designed to minimize this potential obscuration. Section 4.0 summarizes the salient findings and suggests that additional methods be studied to augment the obscuration mitigation effort, particularly in the TDWR environment. Section 5.0 recommends two such methods; i.e., an expanded use of PRF selection and pulse-to-pulse phase modulation. Section 6.0 contains concluding remarks.

2.0 Analysis Description

2.1 Review of Adaptive PRF Selection

TDWR systems will be tasked with identifying short lived, yet extremely hazardous wind shear phenomena known as microbursts, as well as the longer lived phenomena, gust fronts. Microburst surveillance is to occur within the immediate vicinity of the airport runways (typically within a 10 km radius of the airport center), while gust front surveillance covers a much larger geographical area (typically within a 60 km radius). The purpose of the PRF selection technique is to provide two *optimal* PRF values -- one for use while gathering data for microburst surveillance, and the second for use while gathering data for gust front surveillance.

PRF selection is based on an adaptive procedure utilizing measurements of the distant weather situation [7]. At a rate of once every 5 minutes, reflectivity information will be gathered on storm cells within a distance of 460 km from the radar. This distant weather information will be mapped into the available set of PRF values from which will be selected the PRFs for subsequent use. The selection procedure is based on a strategy that seeks to *minimize* the area of range contamination within high priority regions of interest.* Knowledge of the locations of distant weather, coupled with the selected PRF values, enables an accurate prediction of first trip data areas that will subsequently be obscured by range folded echoes. This obscuration information can then be used by an automated editing task to remove *severely* contaminated first trip data from the incoming data stream.

2.2 Analysis Overview

The goals of this investigation were to provide an assessment of the effectiveness of the PRF selection technique at the TDWR testbed and, more importantly, to provide a quantitative assessment of the anticipated effectiveness of the technique within the actual TDWR system. Two analysis capabilities were needed to accomplish these goals: first, a means of quantifying the performance of the technique at the S-Band testbed, and second, a means of extrapolating the results into the C-Band environment. To satisfy these objectives, modifications were made to an off-line version of the PRF selection algorithm.

Figure 2-1 illustrates the basic principles of the PRF selection technique and also introduces the modifications that were necessary for this comprehensive S-Band / C-Band investigation. Here one sees range from the radar plotted as a function of PRF, where the various curves denote first, the unambiguous range interval, followed by nth trip foldover bounds. For purposes of illustration, a high priority region of interest is defined to be from 0 to 25 km from the radar, and the subsequent shaded regions depict nth trip foldover to that region as a function of PRF value.

A hypothetical storm is identified in this figure, centered approximately 200 km from the radar and spreading 10 km in either direction. The PRF selection algorithm maps this storm information into the PRF domain to provide an assessment of obscuration conditions within the high priority region as a function of PRF value. Those PRFs that would result in 2nd trip obscuration from this storm within the high priority region, as well as those PRFs that would result in 3rd trip obscuration, are so indicated. After mapping all such identified storms into the PRF domain, the technique selects that PRF which minimizes the obscuration to the high priority region. (As will be discussed and illustrated later, the technique is further expanded to include obscuration minimization over *multiple* priority zones within a region.)

---

* The data quality degradation in these areas is then based on the relative signal strengths of the first trip and nth trip returns.

PRF values between 600 and 2000 Hz are illustrated in the figure. The operational version of the algorithm at the testbed radar only considers PRFs between 700 and 1220 Hz, as these values represent the available S–Band set. The off–line version of the software, however, was modified to extend the range of available values to 2000 Hz, as the C–Band TDWR PRF set is expected to be a discrete set of values between 1000 and 2000 Hz. This extension essentially provides a means of simultaneously comparing S–Band and C–Band results on the same distant weather data set during off–line analysis.
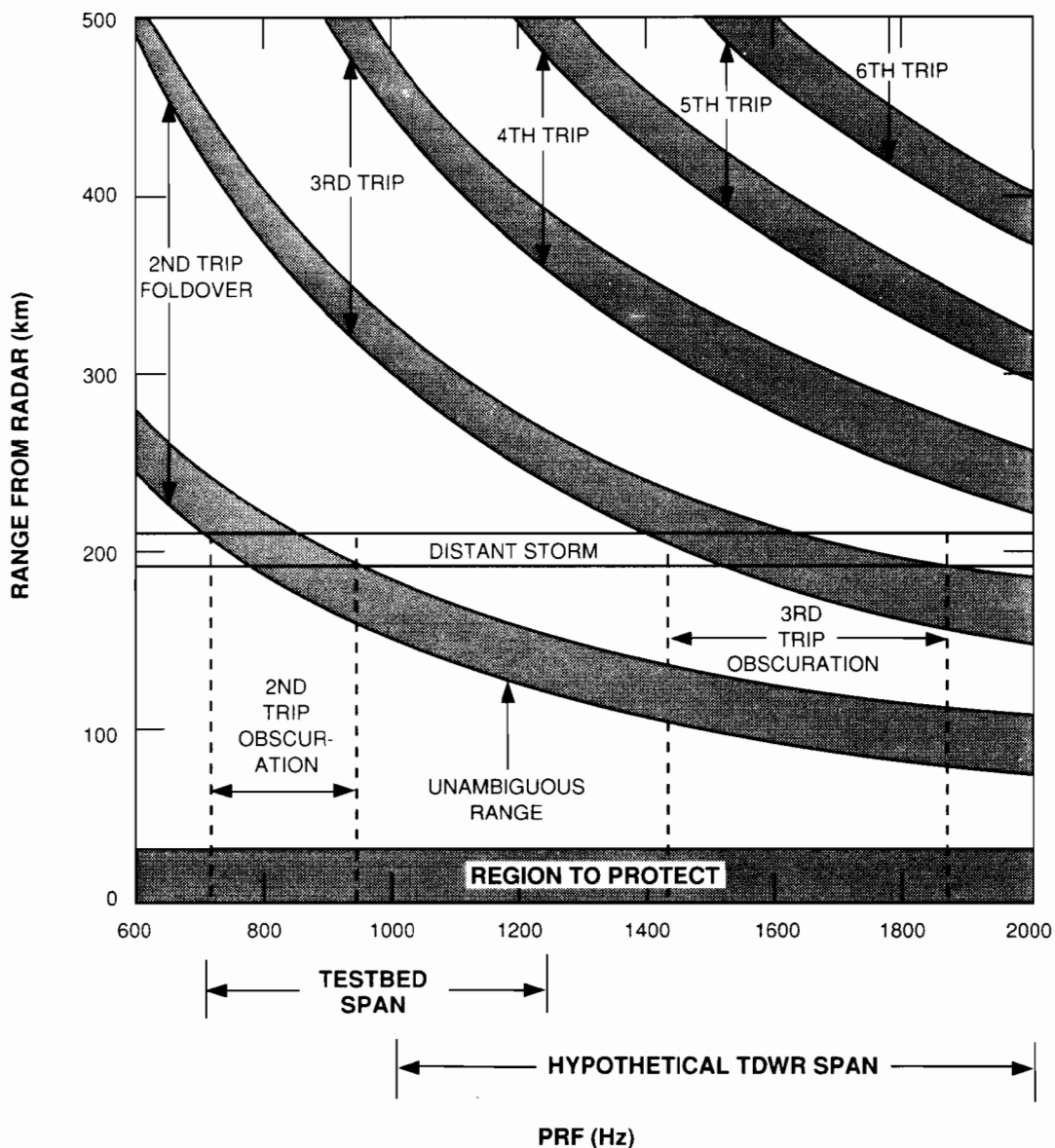
Figure 2-1. Adaptive PRF selection. The intersection of lines containing distant weather with curves defining nth trip foldover bounds indicates which PRF values will result in range contamination to the high priority region.

-4-

2.3 Test Data Set

Every 5 minutes during normal data gathering exercises, the TDWR testbed surveys the distant weather situation using a low elevation, 350 Hz PRF scan ($R = 425$ km) with full 360-deg azimuthal coverage. This information is processed in real time to provide the optimal PRF values which are subsequently used by the testbed, and this information is also stored on magnetic tape for further analysis. The procedure was initiated in June 1987, and a complete distant weather database exists from that time. A set of days from this database was selected, against which to apply the version of the PRF selection algorithm that permits simultaneous comparison of S-Band and C-Band results. (No attempt was made to modify this data set to account for differences posed by collection at the two frequencies; e.g., attenuation by intervening rain.)

The selected set consists of the 15 days identified in Table 1. This set was carefully selected so as to be representative of all types of distant weather and obscuration conditions observed in the Denver area during the hazardous meteorological thunderstorm season; i.e., mild rainshowers to tornadoes. The amount of radar data available on each day (track time) is provided, as is the number of hazardous microburst and gust front events detected within the vicinity of the radar (taken from the weekly testbed summary reports).

Table 1: Selected 1987 Data Set - from Denver, CO -			
Date	Track time (minutes)	No. Microbursts	No. Gust Fronts
12 June	425	27	4
21 June	420	9	4
2 July	580	17	4
16 July	320	4	2
22 July	320	8	2
24 July	480	15	1
2 August	265	4	2
13 August	265	9	2
21 August	355	6	2
24 August	200	5	1
2 September	435	11	4
4 September	355	5	3
9 September	205	3	1
26 September	130	4	2
8 October	155	6	1

2.4 Two Hypothetical Airport Locations

Stapleton Airport is located approximately 15 km northwest of the testbed site, and for Denver operations [8], the microburst surveillance region is considered to be contained within a 120-deg sector out to a range of approximately 35 km from the radar (identified as Sector 1 in Figure 2-2). The gust front surveillance region is contained within a 60 km radius of the testbed location.

Experience has demonstrated that the development and evolution of distant storm structures in the Denver area follow a fairly well established pattern. Small, scattered storm cells typically begin to form over the Rocky Mountains located to the west of Denver. These storms grow in intensity while moving in an easterly direction. The scattered storms then merge to form a fairly large and concentrated mass of shower activity and eventually move out of range of the radar in a southeasterly direction. An example to illustrate this pattern is provided in Section 3.2.3.

As the radar scanned at low elevations toward the direction of the airport, distant weather was partially blocked by the Rocky Mountains. At the higher elevations (above the Rocky Mountains), the distant storms that were observed were typically small and scattered due to their location in the evolutionary storm pattern of the Denver area. To assess the obscuration effects of this geometrical phenomenon, two hypothetical airports were added to the investigation. These airports assumed characteristics of Stapleton runways yet were merely rotated with respect to the testbed location. Obscuration assessment within the vicinity of an airport (real and hypothetical) could then be studied under different geometries and during different phases of a storm's evolution. The location of Stapleton and that of the two hypothetical airports appear in Figure 2-2.

For this analysis, obscuration assessment was conducted in four regions with four PRFs from the S–Band set and four PRFs from the C–Band set being computed at the completion of each PRF update. PRF1_S and PRF1_C (S– and C–Band PRF values, respectively) were selected to minimize obscuration within the microburst surveillance region surrounding Stapleton Airport (i.e., Sector 1). PRF2_S, PRF2_C, PRF3_S, and PRF3_C minimize obscuration within the microburst surveillance regions configured about the hypothetical airports (Sectors 2 and 3), while PRF4_S and PRF4_C minimize obscuration within the gust front surveillance region. The selection process was based on the obscuration minimization criteria provided in [7] and summarized in Section 2.5.1.

PRF Values:	Applicable Region:
PRF1_S, PRF1_C	Sector 1
PRF2_S, PRF2_C	Sector 2
PRF3_S, PRF3_C	Sector 3
PRF4_S, PRF4_C	Gust Front
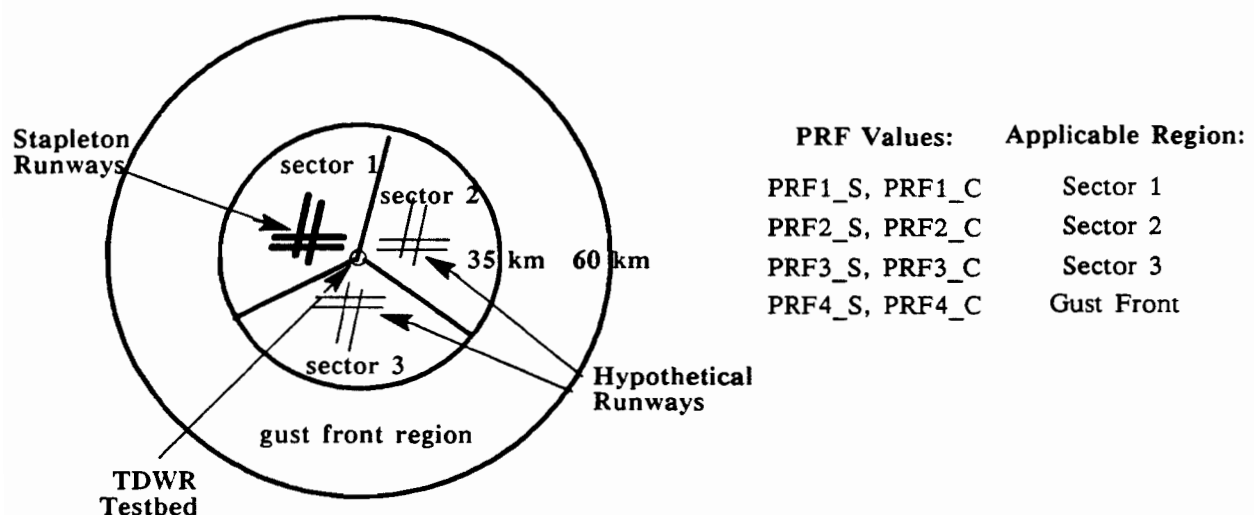
Figure 2-2.   Geometry of airport locations.   Stapleton International Airport, microburst and gust front surveillance regions, and two hypothetical airports with respect to TDWR testbed in Denver, CO.

2.5 Sample Run: June 12, 1987

For each day in the selected set, the modified version of the PRF algorithm was run off–line over the entire track duration. Each distant weather update scan was examined by the modified algorithm, and various intermediate and cumulative results were obtained assuming an S–Band testbed environment and also a C–Band TDWR environment (i.e., a higher set of available PRF values). Examples to illustrate the processing that occurred during this phase of the analysis are provided below. The day selected for illustration is June 12, 1987. (Each of the 15 days in the test set was similarly processed.)

2.5.1 Distant Weather Assessment

Approximately 7 hours of weather data were gathered by the testbed radar on June 12. Once every 5 minutes over the duration of this track, the distant weather scan was conducted. An example of the output of this scan at 2217 UT appears in Figure 2-3.   The PRF selection algorithm is interested in the characteristics of *distant* weather; for the C–Band modification, *distant* weather is any weather beyond 75 km (assuming 2000 Hz is the maximum PRF value), yet less than 425 km. For purposes of algorithm implementation, *distant* weather is further defined to be contained within any radar sampling bin that surpasses a site dependent, season dependent SNR threshold value, typically 7 dB .* As can be seen, several large storm cells and numerous small scattered storm cells make up the distant weather population at that time.

The obscuration mapping function is performed on the distant weather and results in a measure of first trip range obscuration from that weather as a function of PRF value. (This measure is provided in
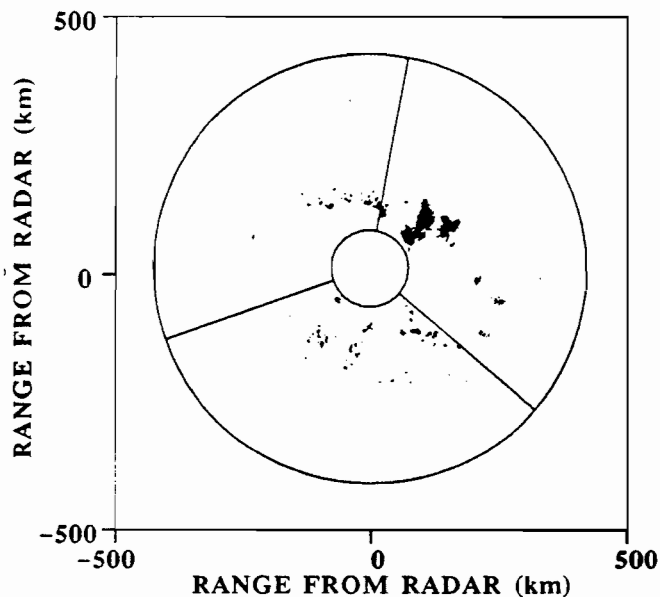
Figure 2-3. Distant weather on June 12, 1987 at 2217 UT. Distant weather within 120-deg sectors affects obscuration assessment in the three respective microburst surveillance regions, while all distant weather affects obscuration assessment in the gust front surveillance region.

---

* 7 dB SNR corresponds to a first trip reflectivity of roughly −8 dBz at the nominal airport range of 15 km.

terms of obscured area.) Figures 2-4 and 2-5 illustrate the results of the mapping procedure on the distant weather under investigation for the S-Band and C-Band PRF sets, respectively, for the microburst surveillance region about Stapleton Airport (i.e., within Sector 1).

Two obscuration profiles are seen for each figure. These two profiles correspond to *two* separate priority zones within the microburst surveillance region that are to be protected; i.e., a zone immediately surrounding the airport runways (roughly 100 sq km in area), and a second zone that encompasses the total microburst surveillance region (roughly 1300 sq km). The selection criteria [7] state that it is of highest priority to minimize obscuration within the airport runway zone. Subject to this constraint, the PRF selection technique subsequently seeks to minimize obscuration over the larger area contained within the microburst surveillance region. Based on this minimization requirement, a PRF value of 818 Hz is selected as *optimal* for the S-Band PRF set, and a value of 1886 Hz is selected as *optimal* for C-Band.

a) Obscuration assessment over
   airport runways.

b) Obscuration assessment over
   120-deg sector.
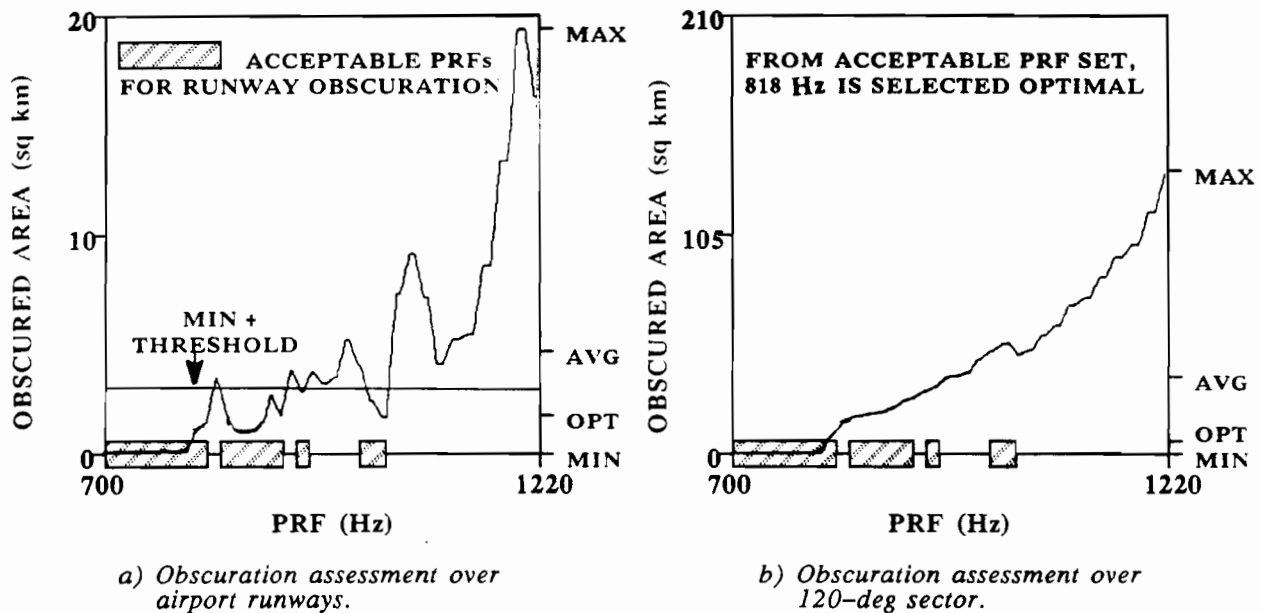
Figure 2-4. June 12 distant weather obscuration assessment at 2217 UT within Sector 1 microburst surveillance region for S-Band PRF set. The minimum obscuration level (in sq km) over airport runways is located. A small threshold is added to the minimum, and all PRF values that result in obscuration less than the modified threshold are considered acceptable. From the acceptable set, that PRF which subsequently minimizes obscuration over the 120-deg sector is selected as optimal.

From each of the obscuration profiles, four values are recorded for further analysis: the *maximum* level of obscuration that could have resulted over the span of available PRF values, the *minimum* level of obscuration, the *average* level of obscuration (averaged over the PRF set), and the *optimal* level of obscuration. (Since the technique seeks to minimize obscuration in *two* separate zones using the same

PRF value, the *optimal* level is not necessarily the *minimum* level.) These four values are identified in Figures 2-4 and 2-5.

a) *Obscuration assessment over airport runways.*

b) *Obscuration assessment over 120-deg sector.*
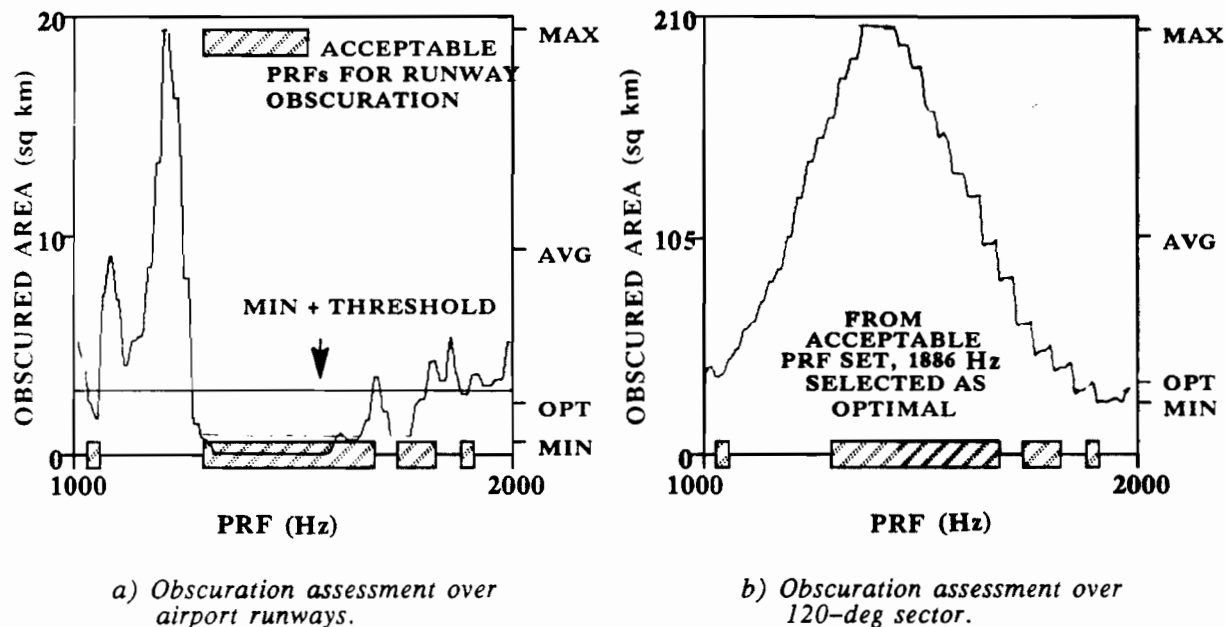
Figure 2-5. June 12 distant weather obscuration assessment at 2217 UT within Sector 1 microburst surveillance region for C-Band PRF set. (PRF selection from this set is as described in Figure 2-4.)

The above example illustrates the obscuration assessment and PRF selection for Sector 1. An identical analysis was performed within Sectors 2 and 3. Similar analysis was performed within the gust front surveillance region, except that the second zone of interest (after the highest priority runway zone) became the gust front surveillance region (i.e., within a 60 km radius of the radar, representing a total area of approximately 11,000 sq km).

2.5.2 Intermediate Track Results

The previous subsection described the processing that occurred for each of the distant weather updates (i.e., once every 5 minutes over the track duration). After processing all distant weather updates for a given day, intermediate results were compiled using the maximum, minimum, average, and optimal obscuration values that were determined at each update. Figure 2-6 illustrates this processing step for the two zones of interest (i.e., the airport runways and the 120-deg sector) within the Sector 1 microburst surveillance region over the duration of the June 12 track, assuming a C-Band PRF scenario.

Four curves are seen in Figures 2-6 (a) and 2-6 (b): curve A plots the variation in the maximum obscuration over the 7 hours of the June 12 track; curve B shows the variation in the minimum obscuration; curve C illustrates the average obscuration; and curve D illustrates the variation in the obscuration that resulted when the optimal PRF value was selected; i.e., that PRF which minimizes *both* zones according to [7].
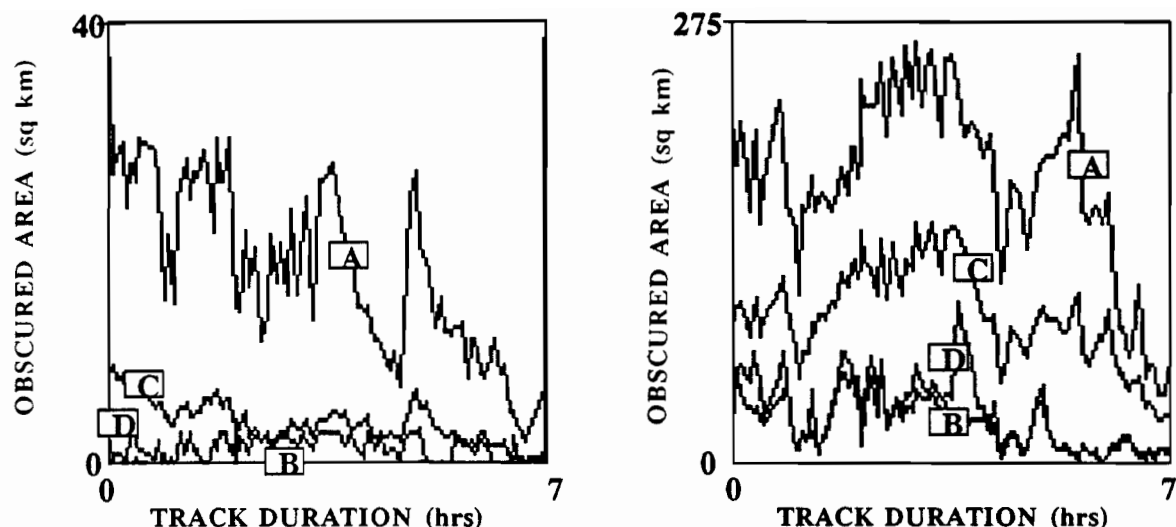
a) Variation in obscuration levels
over the airport runways.

b) Variation in obscuration levels
over the 120-deg sector.

Figure 2-6. Intermediate C-Band obscuration results for both zones of interest (airport runways and 120-deg sector) within Sector 1 microburst surveillance region over duration of June 12 track. Curve A denotes maximum obscuration, curve B denotes minimum obscuration, curve C denotes average obscuration and curve D denotes obscuration level after adaptive PRF selection (i.e, optimal obscuration).

2.5.3 Cumulative Track Statistics

Cumulative compilations of the four curves introduced above, when properly scaled, permit an assessment of the overall effectivess of the technique for the day in question. Figure 2-7 illustrates the cumulative profiles corresponding to Figure 2-6 (b); i.e., over the total 120-deg microburst surveillance sector. As before, four curves are illustrated: curve A denotes the cumulative maximum obscuration; curve B denotes the cumulative minimum obscuration; curve C denotes the cumulative average obscuration; and curve D denotes the cumulative optimal obscuration. By appropriately scaling the results of these profiles (as was done on the figure), a quantitative measure of the expected level of obscuration and an assessment of the overall effectiveness of the adaptive PRF technique can be obtained.

As indicated in Figure 2-7, for example, the maximum level of potential obscuration to occur over the microburst surveillance region at any given time over the June 12 track* is expected to represent approximately 11% of the total area of the region (11% of 1300 sq km is approximately 145 sq km). The corresponding average level is 6%. With adaptive PRF selection, however, this potential obscuration is reduced to 2%, which is quite close to the minimum achievable level of 1.5%. These are results obtained assuming the C-Band PRF set. The corresponding results over the microburst surveillance region assuming the S-Band PRF set are computed to be 9% (maximum), 3% (average), 1% (optimal), and 0% (minimum).

---

* *The results obtained on June 12 within Sector 1 represent obscuration levels somewhat lower than the norm.*
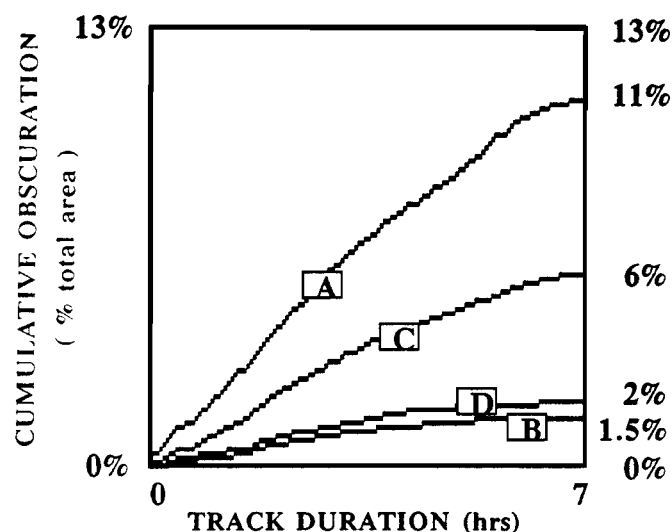
Figure 2-7. Cumulative compilation of C-Band obscuration conditions over the 120-deg Sector 1 microburst surveillance region during June 12 track. Curve A denotes cumulative maximum obscuration, curve B cumulative minimum, curve C cumulative average, and curve D cumulative optimal.

2.5.4 Obscuration Following PRF Selection

The statistics of Section 2.5.3 can be used to provide an assessment of average obscuration conditions following adaptive PRF selection over the duration of the track. (For the C-Band case illustrated in Figure 2-7, this was about 2% of the total area.) The distribution of obscuration conditions *about* that average figure is another parameter of interest, and the amount of time spent in various levels of obscuration following adaptive PRF selection was therefore computed. An example is provided in Figure 2-8, where time distributions of obscuration conditions (in pie-chart format) over Sector 1 airport runways for June 12 are seen for the S-Band and C-Band PRF sets. (The Sector 1 obscuration results, once again, are found to be somewhat lower than the norm.)

a) S-Band Testbed.   *b) C-Band TDWR.*
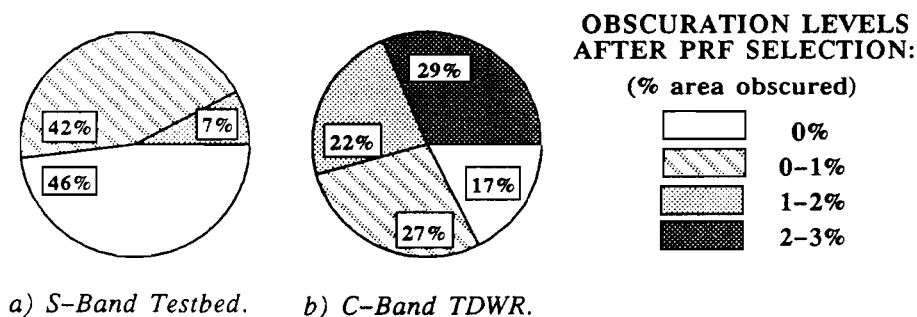
Figure 2-8. Time distribution of S-Band and C-Band obscuration conditions over Sector 1 airport runways following PRF selection (June 12).

2.5.5 PRF Variation

The adaptive PRF technique has been designed to select any integer-valued PRF between 700 and 1220 Hz for subsequent use by the S-Band testbed. The modification for this analysis likewise permitted any integer-valued PRF between 700 and 1220 Hz to be selected as optimal for S-Band and any integer-valued PRF between 1000 and 2000 Hz to be selected as optimal for C-Band. It is of interest to determine how rapidly the PRF values change over the duration of the track (i.e., is the 5-minute update sufficient for obscuration assessment and PRF selection). It is also of interest to examine the distribution of the PRF values selected (i.e., is the distribution uniform across the full range of potential values or is the distribution skewed to lower values, etc.). To answer these questions, the optimal PRF values selected were recorded for further analysis. Plots of PRF values over the duration of the June 12 track appear in Figure 2-9 (a) and (b) for S-Band and C-Band, respectively.

a) S-Band PRF set.
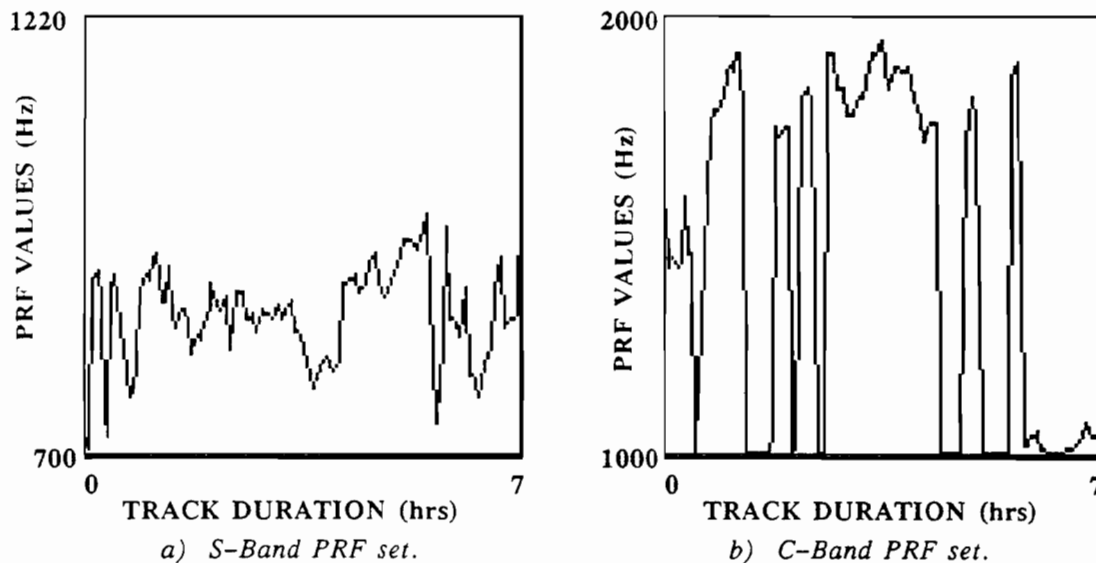
b) C-Band PRF set.

Figure 2-9. PRF variation over duration of June 12 track for S-Band and C-Band PRF sets.

3.0 Analysis Results

3.1 Range Obscuration in Testbed and TDWR Environments

In order to assess the effectiveness of the PRF technique, one must first quantify the amount of obscuration to be dealt with in both the S–Band testbed and C–Band TDWR environments. This assessment is to be based on the analysis of obscuration conditions posed by the 15 days selected from the Denver 1987 distant weather database. While this set of days is considered representative of all types of storms experienced in the Denver area, it still represents only one geographical location. Other areas of the country are expected to experience different distant storm patterns and thus different obscuration conditions. Yet, the analysis to be presented below is considered a reasonable first approximation to general obscuration conditions that may be experienced by the testbed and TDWR systems.

3.1.1 Potential Obscuration for Testbed and TDWR

A method of establishing potential obscuration levels over the duration of a track was introduced in Section 2.5.3. For each of the 15 days of the test data set, Table 2 provides S–Band testbed and C–Band TDWR statistics that were derived by this method. The *maximum* and *average** potential obscuration levels are provided for each of the two zones of interest within the Sector 1 microburst surveillance

	S-Band Testbed				C-Band TDWR			
Date	Runways		120-deg Sector		Runways		120-deg Sector	
	Max	Avg	Max	Avg	Max	Avg	Max	Avg
12 Jun	15	4	9	3	17	4	11	6
21 Jun	13	3	9	4	17	5	10	6
2 Jul	12	3	19	11	16	4	25	15
16 Jul	13	3	5	3	17	5	9	6
22 Jul	5	1	9	3	12	3	11	5
24 Jul	2	<1	3	1	9	2	7	3
2 Aug	7	1	9	2	17	6	12	7
13 Aug	16	6	27	18	21	10	30	21
21 Aug	15	5	11	5	27	10	26	15
24 Aug	23	8	22	14	44	23	42	28
2 Sep	12	4	10	5	24	9	21	11
4 Sep	24	7	16	8	29	12	22	14
9 Sep	6	1	2	1	17	6	12	7
26 Sep	27	9	17	8	29	9	19	10
8 Oct	15	4	7	2	28	10	11	6
Mean:	14	4	12	6	22	8	18	11

Table 2: Potential Obscuration Levels in Sector 1 - percent of total area obscured -

* *The maximum potential level of obscuration would imply that the PRF that results in the greatest amount of obscuration is always selected, whereas the average potential level of obscuration indicates obscuration from a randomly selected PRF value (not the worst, not the best, simply an average).*

-13-

region. (Similar tables that provide results for Sectors 2 and 3 and also for the gust front surveillance region appear in Appendix A.)

3.1.2 Comparison of Testbed and TDWR Potential Obscuration Levels

The arithmetic mean was calculated for each of the columns in Table 2. These mean values appear at the bottom of the table, and can be used to provide a summary of obscuration conditions over all 15 days of the test data set in Sector 1. If one compares the mean values of S-Band entries with the appropriate mean values of C-Band entries, one can assess the differences in obscuration levels posed by operation within the testbed vs TDWR environments. This comparison is provided in Table 3, where clearly one can deduce that an increase in potential obscuration on the order of 50 to 100% is to be expected in the C-Band TDWR environment over that experienced by the S-Band testbed radar. (Similar results are found by examining Tables A-1, A-2 and A-3; i.e., for Sectors 2 and 3 and also the gust front region.)

Table 3: Comparison of S-Band and C-Band Potential Obscuration Levels – percent area obscured –			
	S-Band Testbed	C-Band TDWR	Increase over S-Band
Runways:			
Max obsc.	14%	22%	60%
Avg obsc.	4%	8%	100%
120-deg sector:			
Max obsc.	12%	18%	50%
Avg obsc.	6%	11%	80%

3.2 Effectiveness of Adaptive PRF Selection

Measures of anticipated levels of obscuration were established in Section 3.1. Attention now turns to assessing the effectiveness of adaptive PRF selection in minimizing this potential obscuration.

3.2.1 Average Obscuration Levels Following PRF Selection

Tables 2, A-1, A-2 and A-3 establish the *maximum* and *average* potential levels of obscuration over track duration for each of the 15 days of the selected data set. These tables were derived by analyzing cumulative track profile information introduced in Section 2.5.3. A similar examination of the cumulative profiles is used to provide an assessment of the overall effectiveness of the PRF selection technique for each of the specified days. Table 4 provides the results of this phase of the investigation for each of the 15 days of the data set assuming S-Band and C-Band PRF sets for Sector 1. The level of obscuration that remained after adaptive PRF selection was applied (i.e., *optimal*) appears for both zones of interest within the microburst surveillance region. Table 4 also provides an indication as to how the *optimal* level

compares with the *minimum* level of obscuration.[*]   Similarly computed results for Sectors 2 and 3 and the gust front surveillance region appear in Appendix A.

Table 4: Effectiveness of Adaptive PRF Selection in Sector 1 - percent total area obscured -							
Date	S-Band Testbed				C-Band TDWR			
	Runways		120-deg Sector		Runways		120-deg Sector	
	Opt	Min	Opt	Min	Opt	Min	Opt	Min
12 Jun	1	0	<1	<1	2	<1	2	2
21 Jun	<1	0	<1	<1	1	<1	4	3
2 Jul	1	<1	4	2	1	<1	6	3
16 Jul	<1	0	<1	<1	1	<1	2	2
22 Jul	<1	0	<1	<1	<1	0	<1	<1
24 Jul	<1	0	<1	<1	<1	0	<1	<1
2 Aug	<1	0	<1	<1	<1	<1	1	1
13 Aug	<1	0	3	2	4	2	11	5
21 Aug	1	<1	<1	<1	1	<1	5	2
24 Aug	<1	0	1	1	7	5	19	6
2 Sep	<1	0	<1	<1	2	1	5	3
4 Sep	1	0	2	1	2	1	10	4
9 Sep	<1	0	<1	0	1	<1	<1	<1
26 Sep	<1	0	<1	<1	2	<1	5	4
8 Oct	1	0	<1	0	2	<1	2	2
Mean:	<1	0	<1	<1	2	<1	5	3

3.2.2 Obscuration Distribution Following PRF Selection

The above statistics provide a measure of average performance characteristics of the PRF selection technique, i.e., averaged over track duration and subsequently over data set. These statistics are particularly useful in quantifying the overall effectiveness of adaptive PRF selection in reducing potential range obscuration. The distribution of obscuration conditions following PRF selection *about* the average statistic, however, is also of interest and was computed for further analysis.

Figure 3-1 provides the results of this combined computation for all 15 days of the test data set for Sector 1. Two obscuration distributions are provided in bar-chart format; the first indicates runway obscuration conditions while the second illustrates the conditions within the 120-deg sector. The total track time of the 15 days of this study is determined to be approximately 4900 minutes, and the percent of that time spent in each identified obscuration level is illustrated for the testbed and also for TDWR. (Similar profiles are provided in Appendix A for Sectors 2 and 3 and for the full 360-deg circle.)

---

[*] *The minimum potential level of obscuration would imply that the PRF that results in the least amount of obscuration is always selected. Since the optimal PRF attempts to minimize obscuration simultaneously in two priority zones, minimum levels and optimal levels are not necessarily the same.*
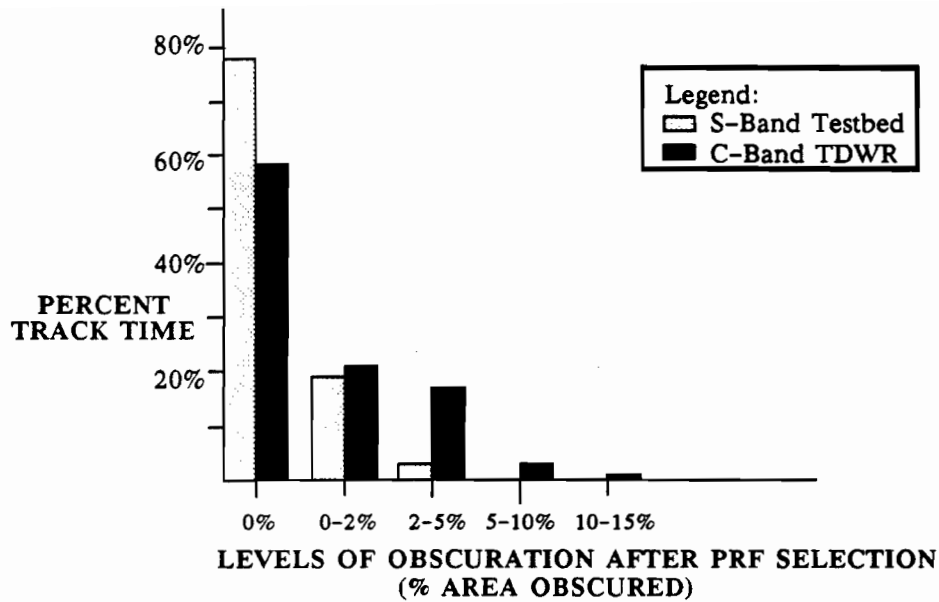
a) Airport runways (total area = 100 sq km).
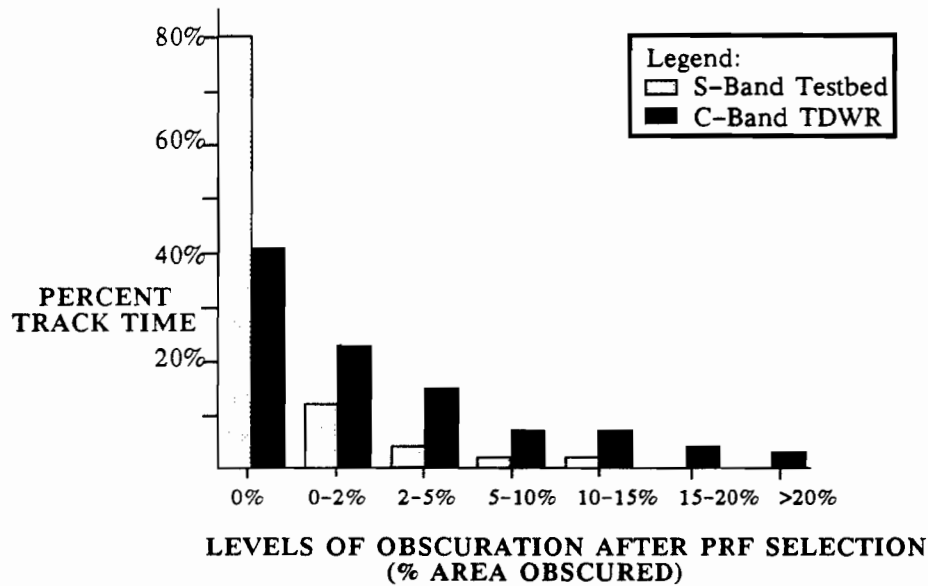
b) 120-deg sector (total area = 1300 sq km)

Figure 3-1. Time distribution over total track time of obscuration conditions within Sector 1 microburst surveillance region. These represent conditions following adaptive PRF selection for runways and 120-deg sector.

3.2.3 Comparison of Results Derived Assuming Alternate Airport Locations

Figures 3-2 (a) through (d) illustrate the time evolution of the storm activity of June 21-22, 1987. Each of these four figures is separated in time by approximately 2 hours. The storm evolution pattern seen here is fairly typical of that observed in the Denver area (previously discussed in Section 2.4).
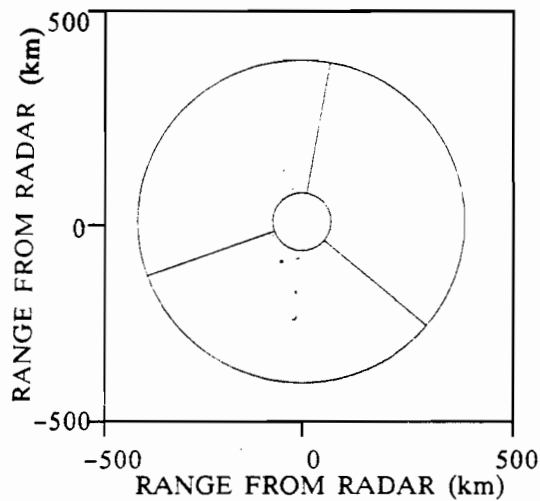
a) *Time = 1827 UT.*
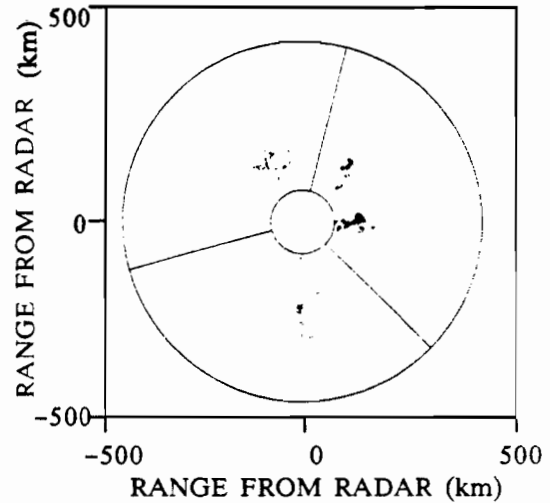
b) *Time = 2033 UT.*
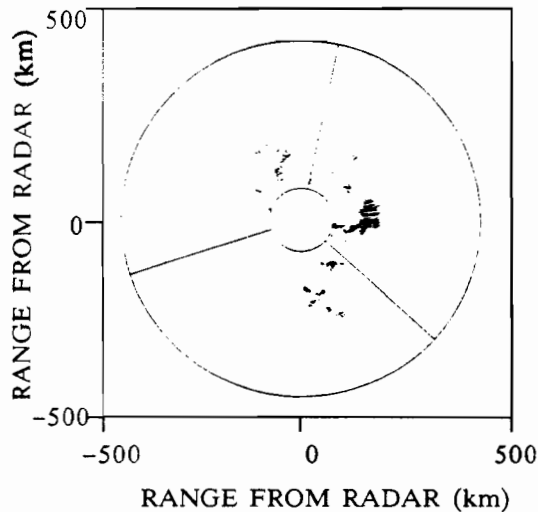
c) *Time = 2203 UT.*
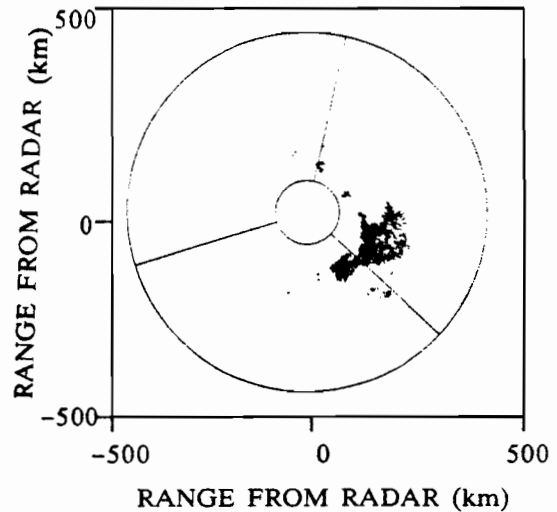
d) *Time = 0055 UT.*

Figure 3-2. Time evolution of June 21, 1987 storm in Denver, CO, as observed by TDWR testbed. Pattern is typical of storm activity in that area.

The storm evolutionary pattern in the Denver area, coupled with the geometrical relationship between the locations of the testbed radar and Stapleton Airport, are considered favorable with respect to minimizing range obscuration within Sector 1. Less distant weather appears in Sector 1 as compared to Sectors 2 or 3 over the course of the storm's development which suggests that obscuration minimization techniques may inherently be more successful in Sector 1 than in the other two sectors. Obscuration is expected to be *least* severe in Sector 1 (i.e., that sector containing Stapleton Airport) and *most* severe in the area identified as Sector 2.

Tables 4, A-4 and A-5 provide a measure of the average obscuration that remains in Sectors 1 through 3, respectively, following adaptive PRF selection for each of the 15 days of the test data set. The mean values of each of the columns in these tables were provided, and offer a mechanism by which to summarize statistics within respective sectors. These mean values appear below in Table 5. Lower levels of obscuration are observed in Sector 1 than in either of the other two sectors for all identified categories (i.e., runways and 120-deg sector for the S-Band testbed, runways and 120-deg sector for the C-Band TDWR). Sector 3 statistics are slightly higher than those of Sector 1, while Sector 2 consistently had the highest obscuration of the three.

Table 5: Comparison of Obscured Area Following PRF Selection - averaged over 15 days -				
Sector	Runways		120-deg Sector	
	S-Band	C-Band	S-Band	C-Band
1	<1%	2%	<1%	5%
2	1%	4%	2%	6%
3	1%	3%	1%	5%

Table 6 examines the time spent under *severe* obscuration conditions, following PRF selection, as a function of sector. (By *severe* is meant that more than 10% of the area under investigation is contaminated by range obscuration.) The results of Sectors 1 and 3 are somewhat comparable, while once again Sector 2 obscuration conditions are consistently worse. These results confirm that there are indeed geometrical variations in performance statistics and suggest that this be a consideration in the future siting of TDWR systems.

Table 6: Comparison of Time Spent in Severe Obscuration - percent of time when obscured area >10% -				
Sector	Runways		120-deg Sector	
	S-Band	C-Band	S-Band	C-Band
1	0%	1%	2%	14%
2	6%	11%	8%	19%
3	0%	5%	1%	8%

3.3 PRF Variation at S-Band and C-Band

For reasons previously discussed, it is of interest to determine the distribution of PRF values calculated for use at the two frequencies. Each PRF value computed for use within Sectors 1 through 3 as well as the gust front region for both S-Band and C-Band was stored for further analysis. This represents approximately 900 such values in each of the various categories, as there were roughly 900 PRF updates over the duration of the 15 days of this study.

Figure 3-3 (a) illustrates the distribution of testbed PRF values that were computed as optimal for use within Sectors 1 through 3. The available set of PRF values (700 – 1220 Hz) is partitioned into 11 categories, each spanning approximately 50 Hz. A noticeable spike of values toward the low end of PRFs (between 700 and 750 Hz) is somewhat to be expected, as these low PRF values provide the largest unambiguous ranges. PRFs appear to be rather uniformly distributed across the 10 remaining categories above 750 Hz, where roughly 8% of the time is expected to be spent using PRFs from each category. Figure 3-3 (b) illustrates the S-Band distribution for the gust front region, where the distribution appears to be more significantly skewed to the lowest span of PRF values. In this figure, for example, PRF values between 700 and 750 Hz are expected to be selected 55% of the time for use by the testbed while collecting data for gust front identification purposes.

a) PRF variation in microburst
    surveillance region.

b) PRF variation in gust front
    surveillance region.

Figure 3-3. Distribution of PRF values from S-Band testbed PRF set (i.e., 700 – 1220 Hz) for use within microburst surveillance region and gust front surveillance region.

Figure 3-4 (a) illustrates the C-Band PRF distribution for the three sectors, while Figure 3-4 (b) provides the distribution for the gust front region. As to be expected, a spike is once again observed in the lowest category of C-Band PRFs (1000 – 1050 Hz) for use within the sectors. Outside this first category, PRF selection appears once again to be somewhat uniform until around 1500 Hz, at which point the distribution gradually tapers to minimal levels. A spike is also observed in the lowest category of PRFs

for the gust front region, which indicates that PRFs between 1000 and 1050 Hz would be selected 40% of the time for use at a C-Band TDWR system for data collection within the gust front region.

a) PRF variation in microburst surveillance region.
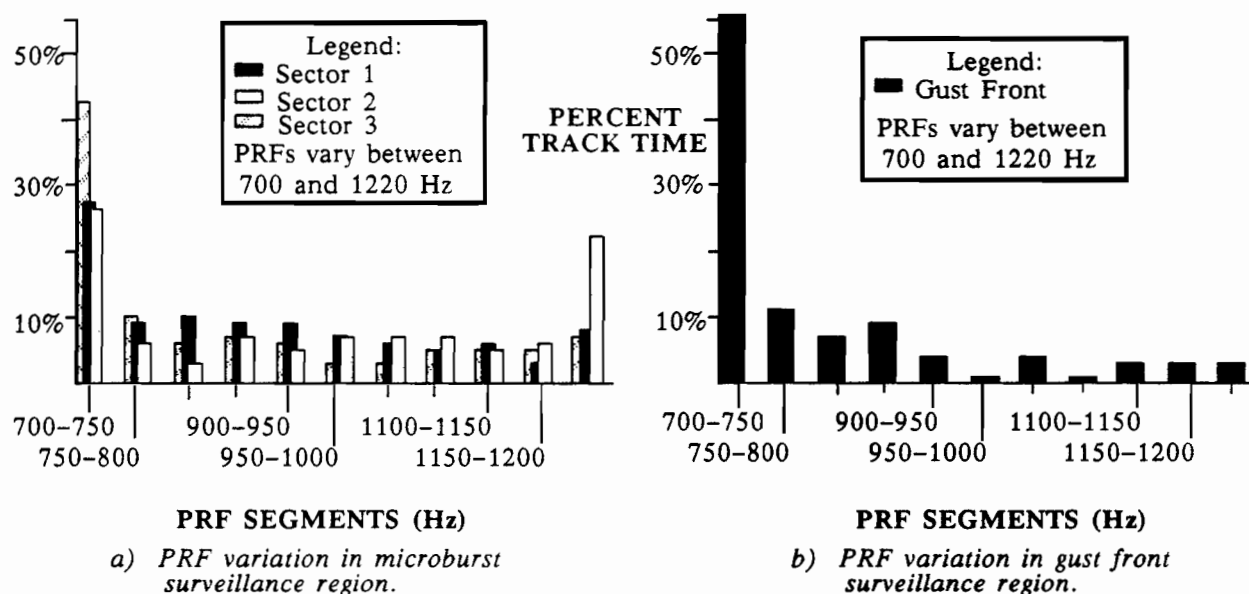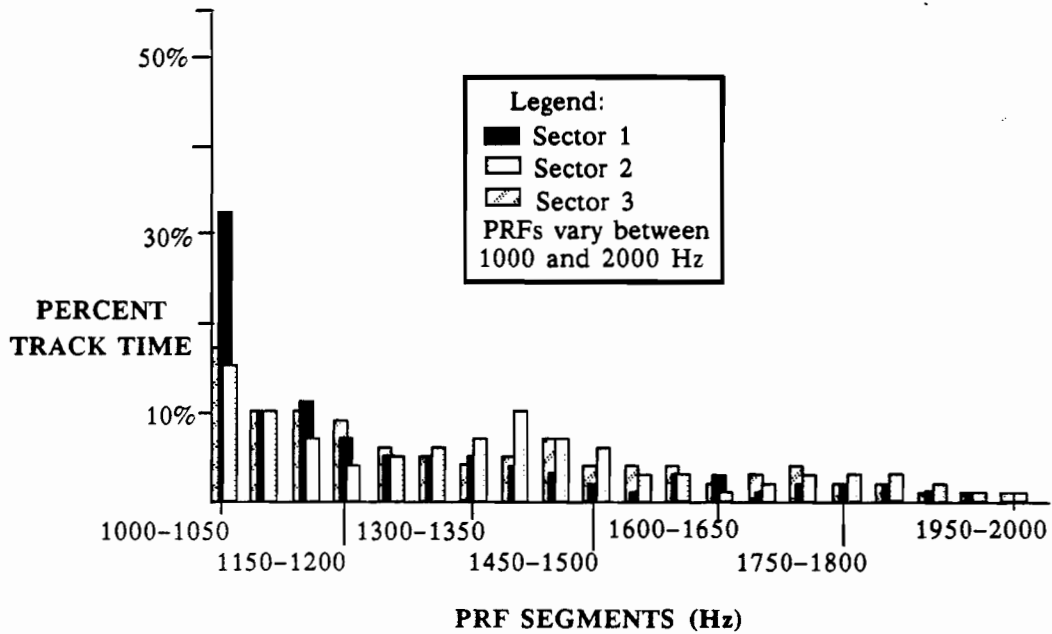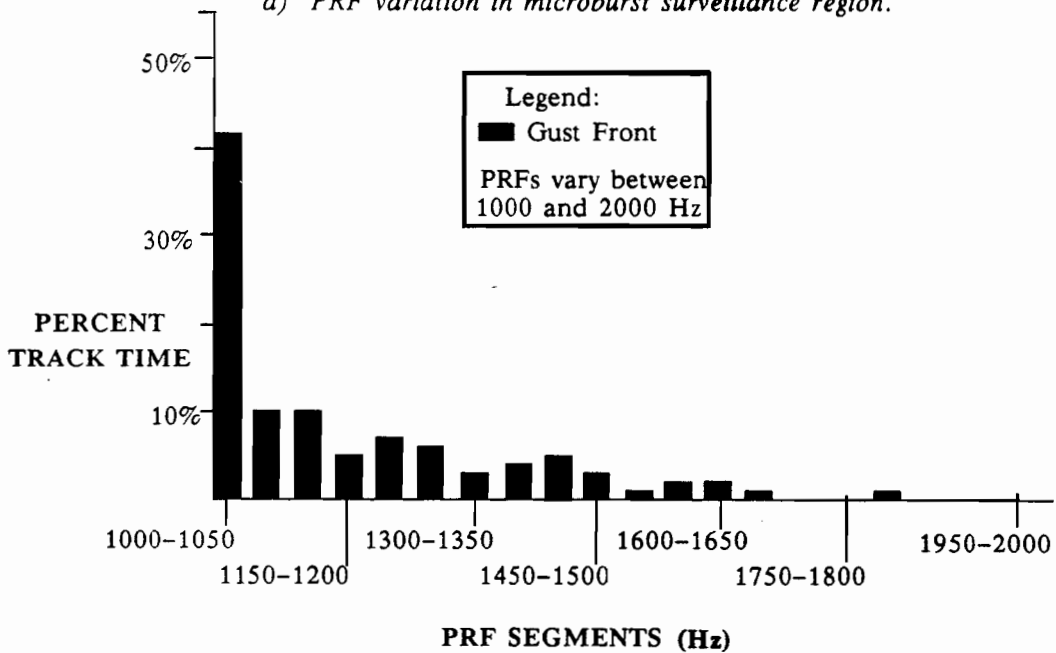

b) PRF variation in gust front surveillance region.

Figure 3-4. Distribution of PRF values from C-Band TDWR PRF set (i.e., 1000 - 2000 Hz) for use within microburst surveillance region and gust front surveillance region.

4.0 Statement of Effectiveness of PRF Selection Technique

The principal goal of this report is to provide a quantitative measure of the effectiveness of the PRF selection technique in minimizing range obscuration for the S–Band testbed radar, and more importantly for the C–Band TDWR system. These results are succinctly provided below in Table 7, which summarizes information introduced and developed in the previous two sections. The PRF selection technique provides two optimal PRF values -- one to be used by the radar while collecting data within the microburst surveillance region, and the second within the gust front surveillance region. The selection strategy is such as to preserve data integrity *first* over the airport runways and *second* within the surveillance region under investigation (i.e., microburst or gust front). Table 7 summarizes the obscuration potential and the effectiveness of the PRF selection strategy in minimizing this potential for the runways and for the two surveillance regions. The potential obscuration levels are provided in terms of the previously defined quantities, *maximum* and *average*. The expected obscuration, following PRF selection is provided in terms of *optimal*, also previously defined. These values have been averaged first over individual track duration; second, over the 15 days of the test data set; and third, over all sectors. (Averaging over the sectors minimizes the bias due to the previously discussed geometrical phenomenon.)

	Runways (100 sq km)			Microburst Surveillance Region (1300 sq km)			Gust Front Surveillance Region (11000 sq km)		
Table 7 Summary of Obscuration Potential and PRF Effectiveness **- percent of area obscured -**									
	Max	Avg	Opt	Max	Avg	Opt	Max	Avg	Opt
S-Band	14%	5%	1%	11%	6%	1%	6%	3%	1%
C-Band	22%	10%	3%	17%	10%	5%	9%	6%	4%

As seen in all categories of the above table, there is a significant reduction in the amount of range obscuration within an area following the application of the adaptive PRF selection technique. The most dramatic reduction is observed within the immediate vicinity of the airport runways, an area in which it is of highest priority to preserve data integrity. In a worst-case scenario, for example, over 20% of this area could be contaminated by range aliased echoes at any given time during TDWR surveillance operations, yet following adaptive PRF selection, this obscuration is reduced to 3%. The corresponding statistics for the testbed are seen to be 14% (maximum) and 1% (optimal).

It has been established that the potential for range obscuration in the TDWR system is expected to be on the order of 50 to 100% greater than that experienced in the S–Band testbed. This claim is clearly supported by comparing results across the two rows of the above table. Since the obscuration potential is higher at C–Band, the obscuration following application of the technique is also higher. While obscuration on the order of 1% is expected in all areas of interest for the S–Band testbed, at C–Band

these levels are seen to be from 3 to 5%, depending on the area.   Clearly, the PRF selection technique can significantly reduce, but not eliminate the problem of range obscuration.

Table 7 provides a mechanism for quantitatively assessing the effectiveness of the PRF selection technique in reducing potential obscuration levels.   Another means by which to analyze performance characteristics of the technique is to examine obscuration conditions following PRF selection over the distribution of total track time.   This information is provided below in pie-chart format in Figure 4-1.

a) Airport runways.

b) 120-deg microburst surveillance region.

c) 360-deg gust front surveillance region.
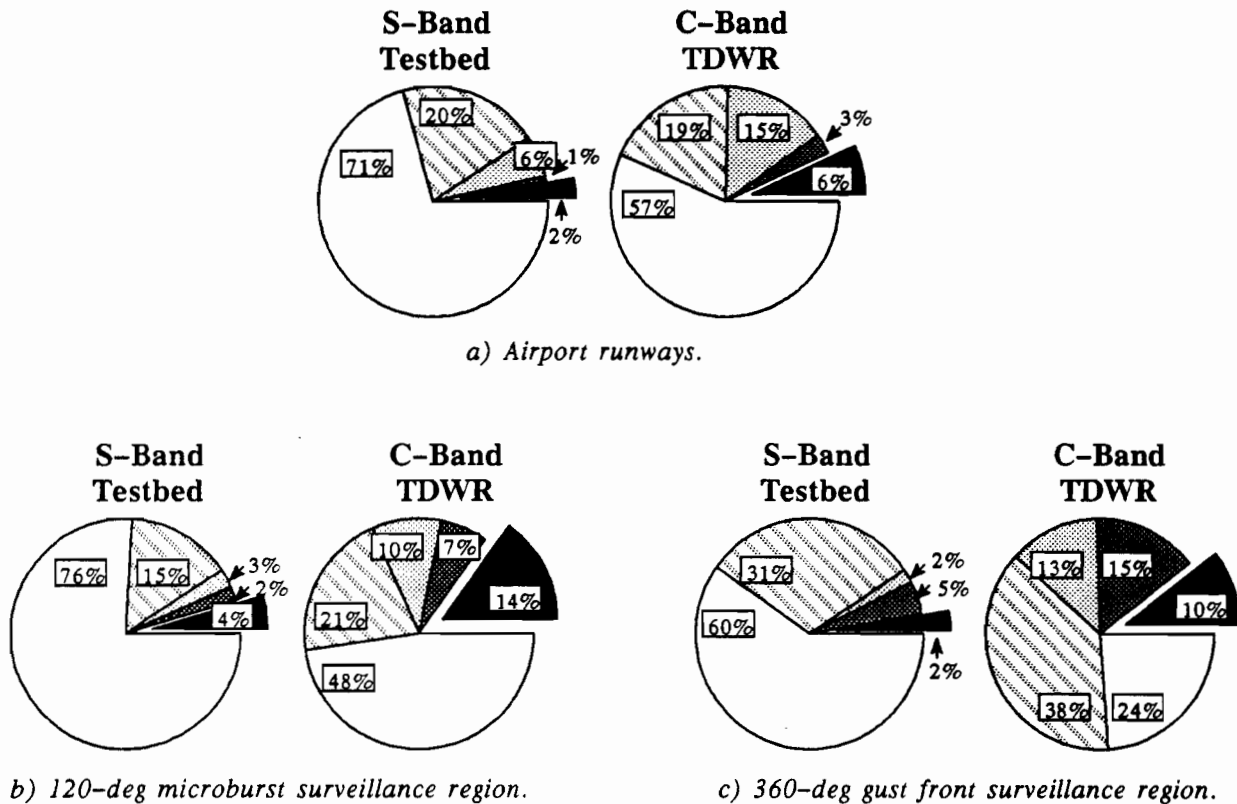
Figure 4-1.   Time distribution of obscuration conditions over airport runways, microburst surveillance region, and gust front surveillance region following adaptive PRF selection for testbed and TDWR.

The three sets of pie charts in Figure 4-1 illustrate the time distribution of obscuration conditions over the airport runways and two surveillance regions. While Table 7 provides information as to average obscuration conditions following PRF selection, these pie charts can be used to assess the distribution about those average conditions. For example, it was previously established that roughly 3% of the area of airport runways is expected to be contaminated with range aliased echoes at any given time during TDWR surveillance operations. Figure 4-1 (a) establishes that no such contamination will exist 57% of the time; between 0 and 2% of the area will be contaminated 19% of the time; between 2 and 5% of the area will be contaminated 15% of the time; between 5 and 10% of the area will be contaminated 3% of the time; and more than 10% of the runway area will be contaminated 6% of the time. The three charts also indicate that the time spent under *severe* levels of obscuration (i.e., more than 10% of the total area is contaminated) is expected to be on the order of between three to five times greater at C-Band than at S-Band.

These charts provide statistics as to the amount of first trip area that will be contaminated with range aliased returns over time following PRF selection. In a number of these cases of contamination, the first trip weather may be sufficiently stronger than the out of trip weather such that no practical problems arise from the contamination. Nevertheless, it appears that additional investigation into techniques for mitigating the effects of range obscuration is warranted at this time.

5.0 Future Obscuration Mitigation Efforts

Table 7 and Figure 4-1 suggest that, while adaptive PRF selection is indeed an effective primary mechanism by which to minimize range obscuration, additional range obscuration mitigation techniques may be required in order for the C-Band TDWR system to be fully effective in its FAA role. Two recommendations are offered that are expected to have significant impact on the overall performance of range obscuration efforts within the S-Band testbed, and more importantly within the C-Band TDWR system. The first deals with a major enhancement to the PRF selection technique itself. This enhancement provides for a expanded use of PRF values, and is expected to further reduce range obscuration levels so as to achieve minimum possible levels of obscuration in the resulting data fields; i.e., using previous notation, the *optimal* level becomes the *minimum* level. Even with this enhancement, however, it is rarely possible to select PRFs that result in zero levels of obscuration. The second recommendation, one of radar phase modulation, provides a means of extracting useful information from those data fields contaminated by range obscuration.

5.1 Expanded Variability in PRF Selection

As previously discussed, the PRF selection technique attempts to simultaneously minimize obscuration over *two* zones of interest; i.e., first the airport runways and subsequently the region under investigation (microburst surveillance region or gust front surveillance region). Figure 5-1 (a) illustrates the currently implemented PRF selection procedure for choosing the optimal PRF value for use within the 120-deg microburst surveillance region, and Figure 5-1 (b) illustrates the procedure for the selection of PRF for use within the gust front surveillance region. It is of highest priority to minimize the obscuration over the airport runways. This area, identified as Priority 1 in both figures, is illustrated as being contained within the indicated wedge. Subject to constraints imposed by this first criterion, the technique

a) *Microburst surveillance region.*
Priority 2 zone is contained within
120-deg sector to range of 35 km.

b) *Gust front surveillance region.*
Priority 2 zone is contained within
360-deg circle to range of 60 km.
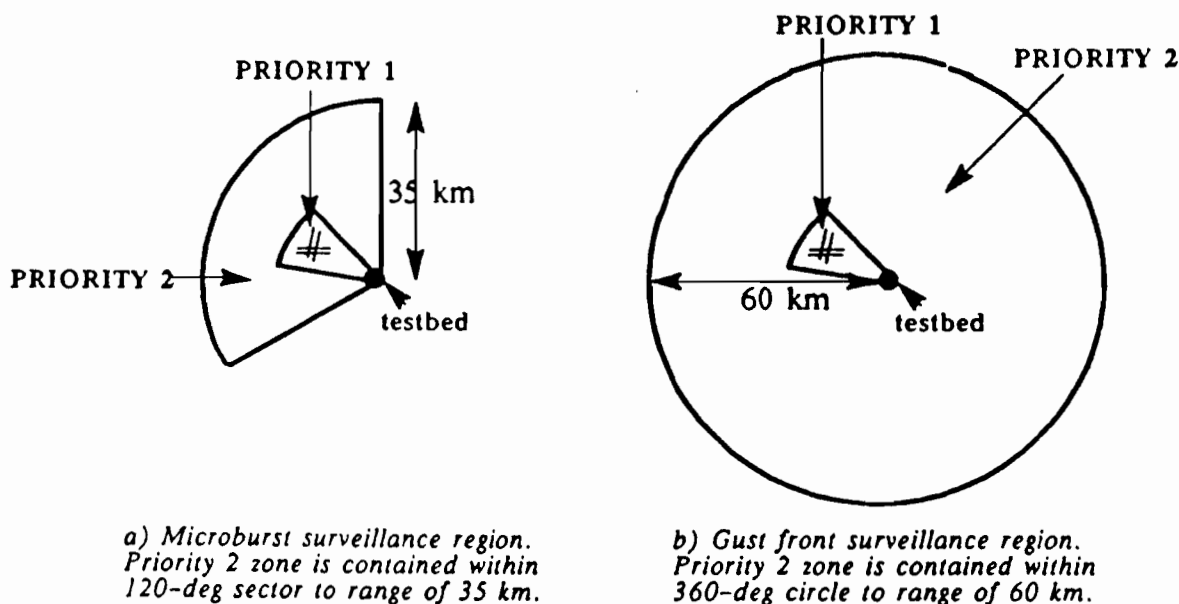
Figure 5-1. Current implementation of PRF selection procedure for microburst and gust front surveillance operations. Priority 1 zone immediately surrounds the airport runways.

then seeks to minimize obscuration within the respective region in general (Priority 2). One PRF value is selected at the completion of the process for use within the microburst surveillance region and this value is used throughout the 120-deg sector. A second PRF is selected for use within the gust front surveillance region, and likewise, this value is used throughout the 360-deg circle. The choice of these values is overwhelmingly dominated by the distant weather conditions beyond the airport runways, here depicted toward the northwest. As a result, obscuration over the runways is minimized, but rarely does this simultaneously result in obscuration within the respective region being minimized. Note, for example, the C-Band results of Table 8 which compare obscuration conditions following PRF selection with minimum possible levels of obscuration. As seen in the table, runway obscuration is expected to be quite close to the minimum achievable level of 2%. The anticipated obscuration within the 120-deg sector, however, at 5% is well above the 2% minimum level possible for this area.

Table 8: Obscuration Following PRF Selection Versus Minimum Achievable Obscuration - percent of area obscured -				
	S-Band Results		C-Band Results	
	Minimum Achievable Obscuration	With PRF Technique	Minimum Achievable Obscuration	With PRF Technique
Runways	<1%	1%	2%	3%
120-deg sector	<1%	1%	2%	5%
360-deg circle	<1%	1%	1%	4%

This proposed enhancement attempts to remove the gap between the expected obscuration levels following adaptive PRF selection and the minimum achievable obscuration levels. Instead of only one PRF value being selected for use within a surveillance region, several values are selected. Each value is specifically chosen to minimize obscuration due to distant weather that lies directly beyond the area where the value will be used. The enhancement is illustrated in Figure 5-2 (a) and (b) for microburst and gust

a) Microburst surveillance region.   b) Gust front surveillance region.

Figure 5-2. Proposed enhancement to PRF selection technique. Multiple PRF values are selected for use within a surveillance region; the selection procedure for segments not containing the airport is based solely on minimizing the area of obscuration within that segment.

front surveillance regions, respectively. In Figure 5-2 (a), the 120-deg microburst surveillance sector is partitioned into three 40-deg segm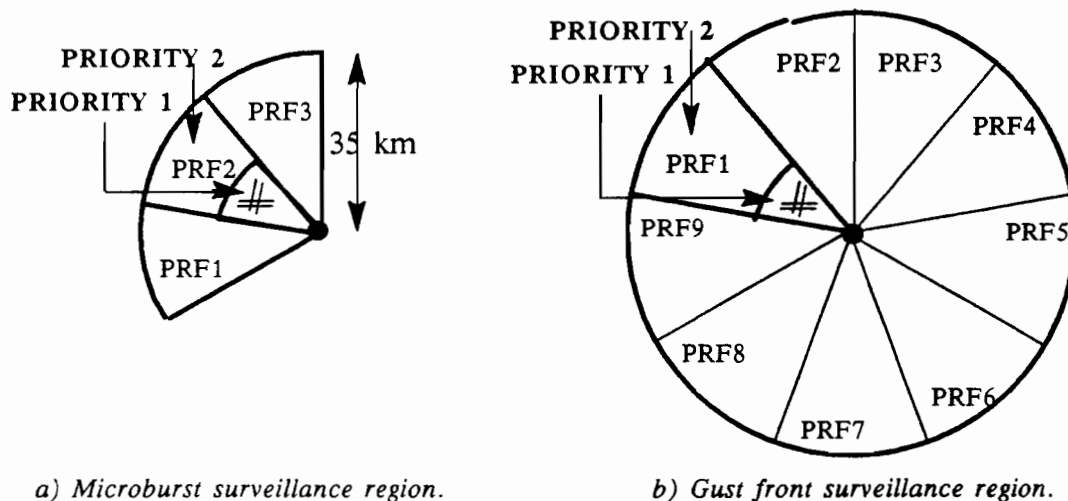ents, and three PRF values are selected for use (identified as PRF1, PRF2, and PRF3). PRF2 will be selected according to [7]; i.e., will be selected so as to minimize obscuration over the runways first, and a much reduced region, second. PRF1 and PRF3 will be selected solely on the basis of minimizing obscuration within the segment. A similar partitioning is observed for the gust front surveillance region. The 40-deg segments are used for illustration only; the best means of partitioning the region is deferred until additional analysis has been performed. In addition, analysis is required as to the effects of this strategy on data quality in those areas abutting PRF crossovers, as, in particular, clutter suppression will undoubtedly be degraded.

5.2 Phase Modulation

Adaptive PRF selection can minimize but not eliminate range contamination. A second recommendation, therefore, offers a means for extracting valid first trip measurement data from range contaminated data fields. The recommendation calls for phase modulation of the outgoing radar pulses. Compensation for this modulation is performed only on the phases of the radar returns associated with objects within the first trip range interval.[*] First trip phases thus remain coherent, while the phases of non-first-trip echoes are de-cohered. The goal is to remove from the radial velocity field those contributions due to non-first-trip weather echoes. Two modulation strategies are currently under investigation at the testbed radar, as described below.

5.2.1 Pseudo-Random Modulation Strategy

B. Laird proposed a pseudo-random approach to the modulation strategy [9] whereby the outgoing pulses are shifted pseudo-randomly by either 0 or 180 deg. This modulation strategy was previously implemented at the testbed and underwent testing by various individuals. One such test examined the effects of the Laird modulation strategy on a known second trip object in the Denver area, i.e., the Cheyenne Ridge. The ridge is located approximately 140 km from the radar, and if PRF values above 1070 Hz are used, the ridge becomes a second trip object. Figure 5-3 illustrates the effects of phase modulation on this second trip object. Two curves are seen; curve A depicts the frequency spectra of the Cheyenne Ridge before phase modulation has been applied, and curve B illustrates the *whitened* spectra that result from the application of pseudo-random phase modulation. The modulation strategy appears to work as expected, yet a recognized shortcoming of the approach is that it significantly raises the noise floor. Whenever the non-first-trip signal dominates that of the first trip (or even whenever the signal strengths become comparable), the increased noise floor may prohibit the extraction of valid first trip measurement data.

5.2.2 Sachidananda/Zrnic' Modulation Strategy

M. Sachidananda and D. Zrnic' [10] offer an alternative approach to that of Laird, and suggest that this alternative may enable valid first trip measurement data to be extracted from range contaminated data fields when the ratio of the first to non-first-trip signal strengths is as low as -15 dB. This may prove to offer an improvement over the previously considered approach.

---

[*]*By phase modulating the coherent local oscillator (COHO), compensation is achieved automatically on received signals and hence no change to the system digital signal processor is required.*
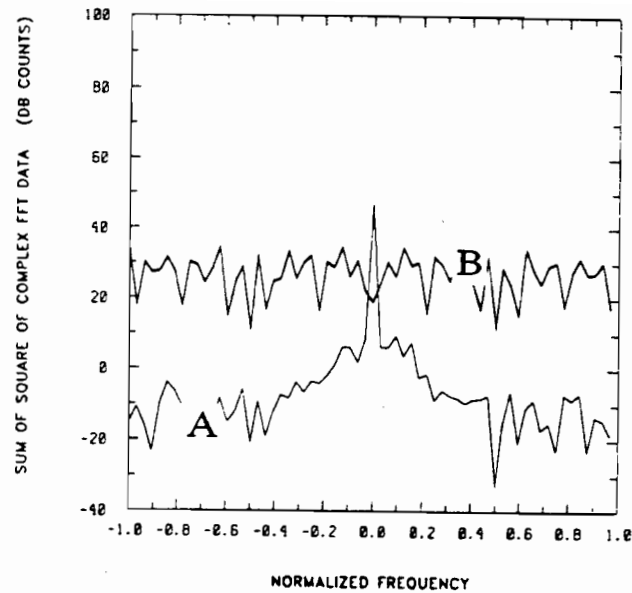
Figure 5-3. Frequency spectra of Cheyenne Ridge before and after pseudo-random phase modulation. Curve A illustrates signature of ridge before modulation; curve B illustrates signature after modulation.

Several modulation strategies with similar properties are proposed by Sachidananda and Zrnic'. The one of particular interest at this time is referred to as the $\pi/2$ technique and consists of a specified sequence of 0 and $\pi/2$ phase shifts. The frequency spectra of this technique are seen in Figure 5-4 from
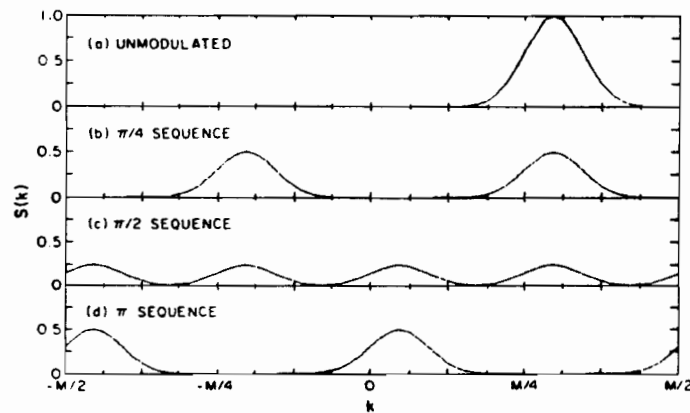
Figure 5-4. Frequency spectra of three phase modulation strategies by M. Sachidananda and D. Zrnic' (from [10]). Curve (a) depicts frequency spectra before phase modulation; curve (b) illustrates spectra after $\pi/4$ phase modulation; curve (c) illustrates spectra after $\pi/2$ phase modulation; and (d) illustrates frequency spectra after π phase modulation.

-27-

[10]. As observed, the modulation strategy *partitions* rather than *whitens* the frequency spectra. Upon pulse pair processing, it can be shown that the contributions from these *partitioned* spectra to a pulse pair mean velocity estimate tend to zero. The $\pi/2$ technique was implemented at the testbed radar during the spring of 1988, and initial reaction has been quite favorable. In fact, the technique, on a limited basis, became part of a TDWR operational demonstration conducted during July and August 1988 at the testbed site. Figures 5-5 (a) through (c) provide an example of its operational use.

Figure 5-5 (a) illustrates processed reflectivity data to a distance of approximately 100 km from the testbed location at 2223 UT on August 23, 1988. Clearly, the signature of a non-first-trip weather echo is present to the east of the radar, contaminating a significant portion of the data. Figure 5-5 (b) shows the corresponding velocity field before the $\pi/2$ modulation strategy was invoked, where once again a clear signature of the non-first-trip echo is seen. Figure 5-5 (c) illustrates the effects within the velocity field after phase modulation of the outgoing pulses by the $\pi/2$ sequence. Of particular interest in this figure is the fact that the underlying signatures of the first trip weather data (predominantly green in color) appear to emerge, even in the presence of significant contamination by the non-first-trip source. These results are extremely encouraging, and phase modulation techniques of this type are receiving special attention at the testbed radar site at this time.

time: 88/08/23 22:27:56 0.5 degrees

1	
45 dBZ	
40 dBZ	
35 dBZ	
30 dBZ	
25 dBZ	
20 dBZ	
15 dBZ	
10 dBZ	
5 dBZ	
0 dbZ	
-5 dBZ	
-10 dBZ	
-15 dBZ	
bad	

TDWR
TESTBED >

TDWR
TESTBED >

(a) Reflectivity data to distance of 100 km from TDWR testbed.

time: 88/08/23 22:27:56 0.5 degrees

(b) Radial velocity data to distance of 100 km before phase modulation invoked.

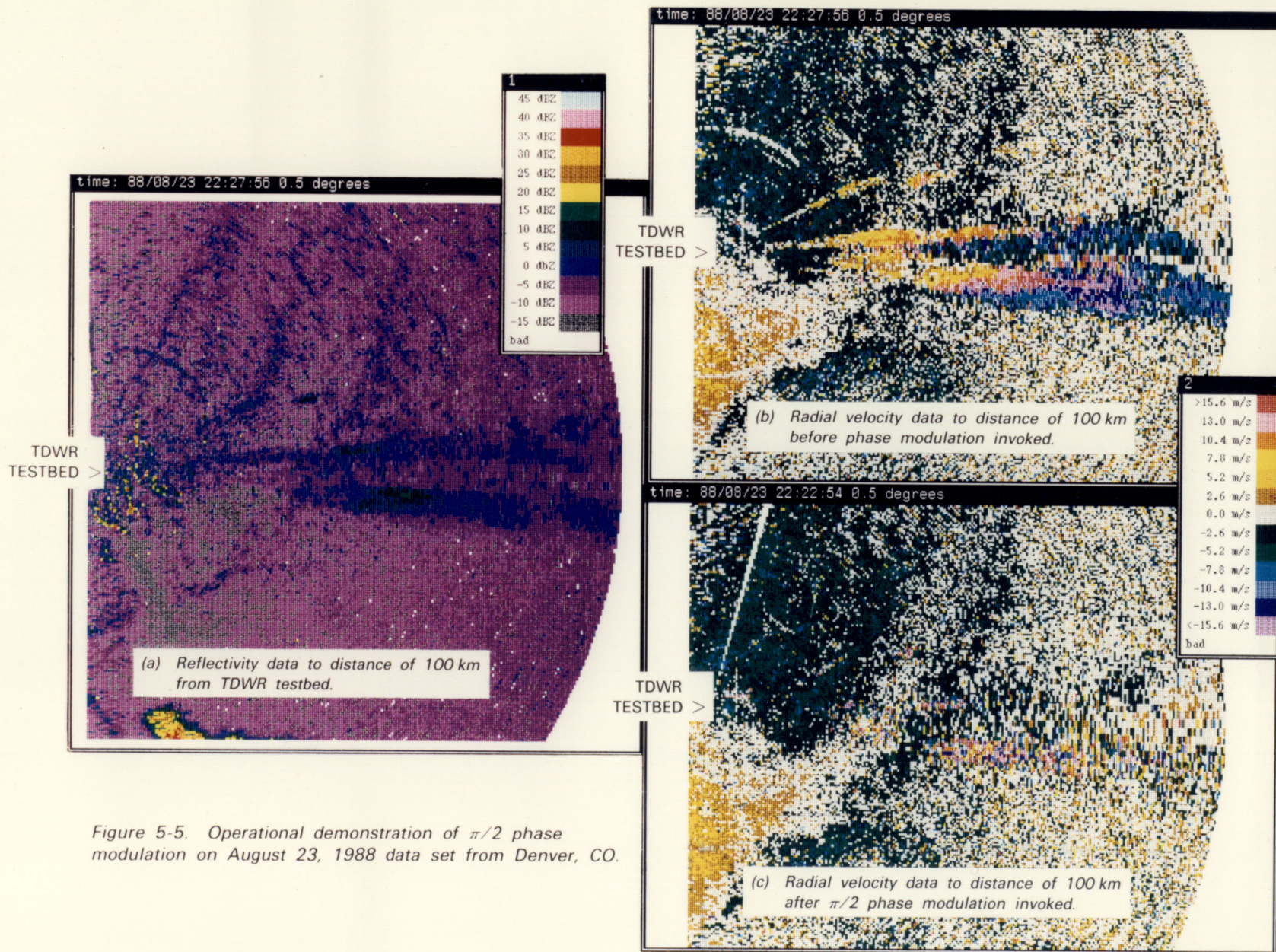| 2	
>15.6 m/s	
13.0 m/s	
10.4 m/s	
7.8 m/s	
5.2 m/s	
2.6 m/s	
0.0 m/s	
-2.6 m/s	
-5.2 m/s	
-7.8 m/s	
-10.4 m/s	
-13.0 m/s	
<-15.6 m/s	
bad	

time: 88/08/23 22:22:54 0.5 degrees

TDWR
TESTBED >

Figure 5-5. Operational demonstration of $\pi/2$ phase modulation on August 23, 1988 data set from Denver, CO.

(c) Radial velocity data to distance of 100 km after $\pi/2$ phase modulation invoked.

6.0 Conclusion

A procedure has been developed for adaptively selecting the pulse repetition frequency for the TDWR system. The goal of this selection procedure is to minimize the occurrence of range aliased echoes over the operationally significant coverage areas of the system. This procedure has undergone extensive testing in the S–Band TDWR testbed. The purpose of this report is to provide a quantitative assessment of the anticipated performance of the technique within a C–Band TDWR system, where an increase in obscuration potential on the order of 50 to 100% is expected over that experienced within the S–Band testbed. To provide such an assessment, an extensive object data set was introduced, analysis methods were fully described, and examples to illustrate all levels of data processing were presented.

Salient findings of this analysis, as succinctly provided in Table 7, suggest that the technique is indeed quite effective as the primary tool in the range obscuration mitigation effort. Without PRF selection, for example, as much as 22% of all data collected in the immediate vicinity of the airport runways could be contaminated with range aliased echoes at any given time during normal TDWR surveillance operations. This level of obscuration would seriously degrade TDWR system performance characteristics. With PRF selection, however, the level of expected obscuration is reduced to approximately 3% of all data.

The PRF selection technique can minimize range obscuration in the TDWR system, but not necessarily eliminate the problem altogether. On average, 3% of the data is expected to be contaminated over the airport runways during TDWR surveillance operations. The distribution of obscuration conditions about that average figure, as seen in Figure 4–1, indicates there will be occasions when significant obscuration will exist even with PRF selection. Large distant storm patterns move into a region in such a way as to cause obscuration conditions about operationally significant areas no matter what the selected PRF value. Section 3.2.3 suggests that future TDWR siting studies include an investigation into evolutionary storm patterns in an area so as to minimize the potential for this occurrence.

Adaptive PRF selection has been found extremely effective in its ability to preserve data integrity over the airport runways. An enhancement to the technique, which calls for an expanded use of PRF values outside the immediate vicinity of the runways, is recommended as a means to further improve data integrity over larger TDWR surveillance areas (i.e., outside the immediate vicinity of the runways). This enhancement should result in minimum achievable levels of obscuration in *all* areas of TDWR surveillance, not just the airport runways.

A second recommendation set forth in this report stipulates the use of radar phase modulation in conjunction with adaptive PRF selection to augment the TDWR range mitigation effort. Phase modulation offers a means by which to extract valid first trip velocity measurement data from those areas where range contamination is present. An example of the performance of this type of technique, using TDWR testbed data, was provided.

REFERENCES

[1] Doviak, R.J. and D.S. Zrnic', *Doppler Radar and Weather Observations*, Academic Press, Inc., Orlando, FL, 1984.

[2] Skolnick, M.I., *Introduction to Radar Systems*, 2nd Edition, McGraw-Hill Inc., New York, 1980.

[3] Evans, J.E. and D. Johnson, *The FAA Transportable Doppler Weather Radar*, 22nd AMS Conference on Radar Meteorology, Zurich, pp. 246–250, 1984.

[4] Campbell, S.D. and M.W. Merritt, *Advanced Microburst Recognition Algorithm*, MIT Lincoln Laboratory Project Report ATC-145, to be published.

[5] Klingle-Wilson, D. et. al., *Gust Front Detection Algorithm for the Terminal Doppler Weather Radar, Part 2: Performance Assessment*, preprints, Third International Conference on the Aviation Weather System, January 1989, AMS, Boston, MA.

[6] Terminal Doppler Weather Radar Specification, U.S. Department of Transportation, Federal Aviation Administration, FAA-E-2806.

[7] Crocker, S.C., *TDWR PRF Selection Criteria*, MIT Lincoln Laboratory Project Report ATC-147, 15 March 1988.

[8] Campbell, S.D. and M.W. Merritt, *TDWR Scan Strategy Requirements*, MIT Lincoln Laboratory Project Report ATC-144, 3 November, 1988.

[9] Laird, B.G., *On Ambiguity Resolution by Random Phase Processing*, in 20th AMS Conference on Radar Meteorology, Boston, MA, pp. 327–331, 1981.

[10] Sachidananda, M. and D. Zrnic', *Recovery of Spectral Moments from Overlaid Echoes in a Doppler Weather Radar*, IEEE Trans. on Geoscience and Remote Sensing, Vol. GE-24, No. 5, September 1986.

Appendix A: Obscuration Assessment in Alternate Regions

Table 2 in Section 3.1.1 established potential obscuration levels for Sector 1 over the duration of individual tracks for each of the 15 days of the data set. Tables A-1 and A-2 provide this information for Sectors 2 and 3, respectively, while Table A-3 provides potential obscuration levels for the gust front region.

Table A-1: Potential Obscuration Levels in Sector 2 - percent of total area obscured -							
Date	S-Band Testbed				C-Band TDWR			
	Runways		120-deg Sector		Runways		120-deg Sector	
	Max	Avg	Max	Avg	Max	Avg	Max	Avg
12 Jun	20	10	15	9	27	15	24	15
21 Jun	35	17	26	16	43	21	32	23
2 Jul	43	26	48	35	64	41	67	50
16 Jul	3	<1	4	2	7	1	6	3
22 Jul	2	<1	5	1	9	2	12	5
24 Jul	2	<1	1	<1	4	<1	3	1
2 Aug	5	1	5	2	12	3	6	3
13 Aug	11	2	8	4	21	9	14	7
21 Aug	17	6	12	4	28	18	30	20
24 Aug	3	<1	2	1	4	<1	4	2
2 Sep	3	1	8	4	13	6	16	7
4 Sep	34	21	29	20	41	27	33	26
9 Sep	<1	<1	<1	<1	1	<1	3	1
26 Sep	1	<1	4	2	2	<1	5	2
8 Oct	1	<1	1	<1	1	<1	3	1
Mean:	12	6	11	7	18	10	17	11

Table A-2: Potential Obscuration Levels in Sector 8
- percent of total area obscured -

Date	S-Band Testbed				C-Band TDWR			
	Runways		120-deg Sector		Runways		120-deg Sector	
	Max	Avg	Max	Avg	Max	Avg	Max	Avg
12 Jun	8	2	5	2	21	8	11	7
21 Jun	13	3	13	5	16	5	17	9
2 Jul	10	1	6	2	15	3	10	5
16 Jul	6	1	4	2	11	3	6	3
22 Jul	6	1	7	4	14	4	11	6
24 Jul	15	5	14	7	25	9	8	5
2 Aug	27	13	16	9	37	21	23	16
13 Aug	28	14	18	10	44	29	30	20
21 Aug	13	4	7	3	37	18	23	11
24 Aug	19	9	11	6	27	12	24	13
2 Sep	23	9	11	7	31	13	18	10
4 Sep	17	5	10	4	23	9	13	8
9 Sep	17	3	6	3	25	8	14	6
26 Sep	3	<1	1	<1	13	3	3	1
8 Oct	46	20	25	9	51	25	30	19
Mean:	17	6	10	5	26	11	16	9

Table A-3: Potential Obscuration Levels in Gust Front Region
- percent of total area obscured -

Date	S-Band Testbed				C-Band TDWR			
	Runways		360-deg Circle		Runways		360-deg Circle	
	Max	Avg	Max	Avg	Max	Avg	Max	Avg
12 Jun	15	4	5	2	18	4	8	6
21 Jun	13	3	8	5	17	5	11	9
2 Jul	12	3	14	10	16	4	20	15
16 Jul	13	3	2	1	17	5	3	2
22 Jul	5	1	3	2	12	3	5	3
24 Jul	2	<1	2	1	9	2	4	2
2 Aug	7	1	5	2	17	6	7	5
13 Aug	16	6	9	6	21	10	14	10
21 Aug	15	5	5	2	27	10	14	8
24 Aug	23	8	7	4	44	23	13	8
2 Sep	12	4	5	3	24	9	9	5
4 Sep	24	7	10	6	29	12	13	10
9 Sep	6	1	1	1	17	6	5	2
26 Sep	27	9	4	2	29	9	4	3
8 Oct	15	4	5	2	28	10	8	6
Mean:	14	4	6	3	22	8	9	6

Table 4 in Section 3.2.1 provides an assessment of the effectiveness of adaptive PRF selection within Sector 1 for each of the 15 days of the data set. Tables A-4 and A-5 provide this information for Sectors 2 and 3, respectively, while Table A-6 provides this information for the gust front region.

| Table A-4: Effectiveness of Adaptive PRF Selection in Sector 2 - percent total area obscured -							
Date	S-Band Testbed				C-Band TDWR			
	Runways		120-deg Sector		Runways		120-deg Sector	
	Opt	Min	Opt	Min	Opt	Min	Opt	Min
12 Jun	3	2	3	2	6	5	9	3
21 Jun	<1	0	2	1	2	1	18	4
2 Jul	11	10	25	4	20	18	35	4
16 Jul	<1	0	<1	<1	<1	0	1	<1
22 Jul	<1	0	<1	0	<1	0	<1	<1
24 Jul	<1	0	<1	<1	<1	0	<1	<1
2 Aug	<1	0	<1	<1	1	0	1	1
13 Aug	<1	0	<1	<1	2	<1	3	2
21 Aug	<1	0	<1	<1	7	6	6	1
24 Aug	<1	0	<1	<1	<1	0	<1	<1
2 Sep	<1	<1	<1	<1	1	<1	2	1
4 Sep	6	5	4	2	16	15	19	2
9 Sep	0	0	<1	0	<1	0	<1	0
26 Sep	<1	0	<1	<1	<1	0	1	1
8 Oct	<1	0	<1	0	<1	0	<1	<1
Mean:	1	1	2	<1	4	3	6	1

Table A-5: Effectiveness of Adaptive PRF Selection in Sector 3
- percent total area obscured -

| Date	S-Band Testbed				C-Band TDWR			
	Runways		120-deg Sector		Runways		120-deg Sector	
	Opt	Min	Opt	Min	Opt	Min	Opt	Min
12 Jun	<1	0	<1	<1	1	<1	2	1
21 Jun	1	0	1	1	1	0	2	2
2 Jul	<1	0	<1	<1	<1	0	2	1
16 Jul	1	0	<1	<1	1	0	1	1
22 Jul	1	<1	1	1	1	<1	3	3
24 Jul	1	<1	1	2	1	<1	2	1
2 Aug	1	<1	1	1	8	6	11	5
13 Aug	4	3	3	2	13	12	10	6
21 Aug	1	<1	<1	<1	3	2	3	2
24 Aug	2	<1	1	1	3	1	4	3
2 Sep	1	<1	3	2	3	1	5	3
4 Sep	1	0	<1	<1	3	1	5	3
9 Sep	1	0	<1	<1	2	<1	1	1
26 Sep	<1	0	<1	0	<1	0	<1	<1
8 Oct	1	0	<1	<1	9	6	17	6
Mean:	1	<1	1	<1	3	2	5	3

Table A-6: Effectiveness of Adaptive PRF Selection in Gust Front Region
- percent total area obscured -

Date	S-Band Testbed				C-Band TDWR			
	Runways		360-deg Circle		Runways		360-deg Circle	
	Opt	Min	Opt	Min	Opt	Min	Opt	Min
12 Jun	<1	0	1	<1	2	<1	4	1
21 Jun	1	0	1	<1	1	<1	6	1
2 Jul	1	<1	6	1	1	<1	10	1
16 Jul	<1	0	<1	<1	1	<1	1	1
22 Jul	<1	0	1	1	<1	0	1	1
24 Jul	<1	0	1	<1	<1	0	1	<1
2 Aug	<1	0	1	<1	<1	<1	2	1
13 Aug	1	0	1	1	3	2	8	1
21 Aug	1	<1	<1	<1	1	0	3	<1
24 Aug	<1	0	<1	<1	7	5	5	1
2 Sep	<1	0	1	<1	2	1	4	1
4 Sep	1	<1	1	1	2	1	8	1
9 Sep	0	0	<1	<1	1	<1	1	<1
26 Sep	<1	0	<1	<1	3	<1	2	1
8 Oct	0	0	<1	<1	1	<1	3	1
Mean:	<1	<1	1	<1	2	<1	4	1

Figures 3-1 (a) and (b) from Section 3.2.2 illustrate the time distribution over total track time of obscuration conditions within Sector 1 for the airport runways and 120-deg microburst surveillance region, respectively. Figures A-1 and A-2 provide similar information for Sectors 2 and 3, respectively, while Figure A-3 provides the information for the gust front region.
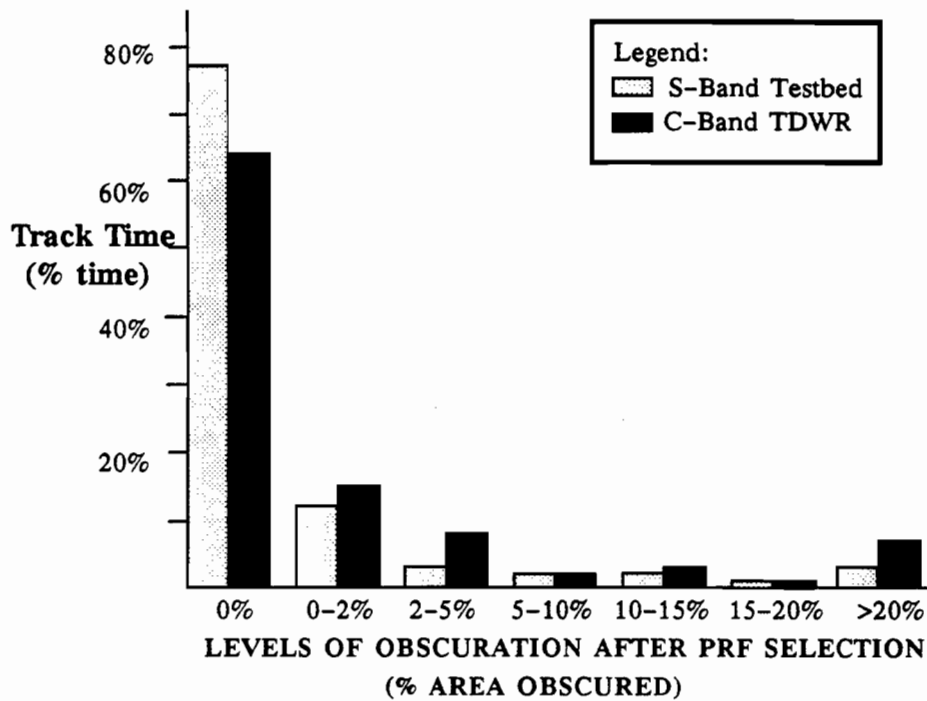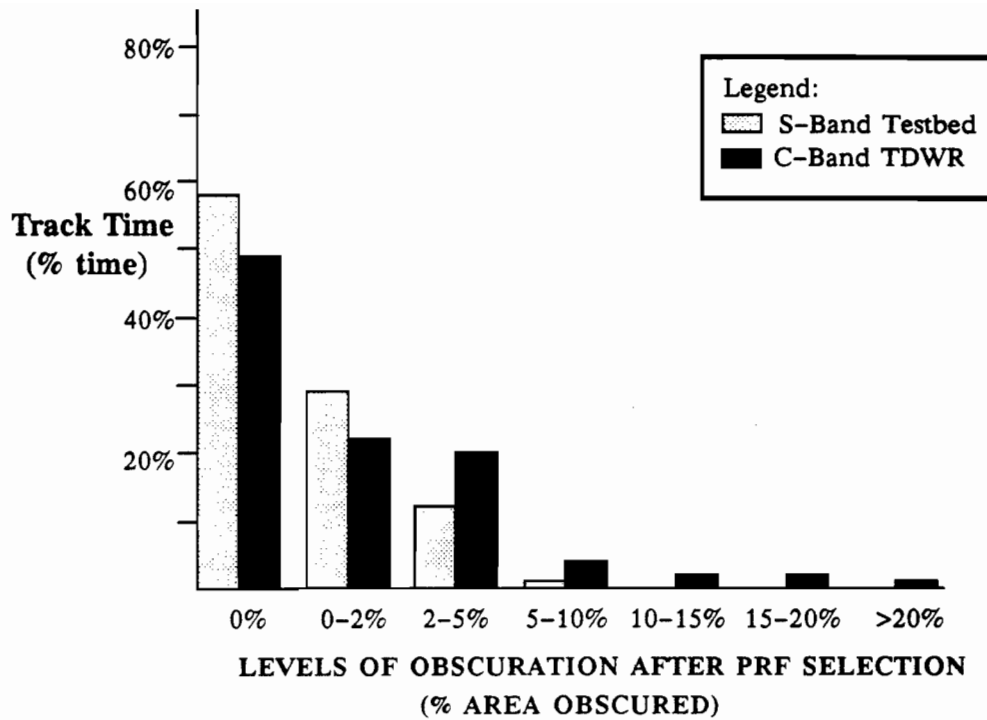
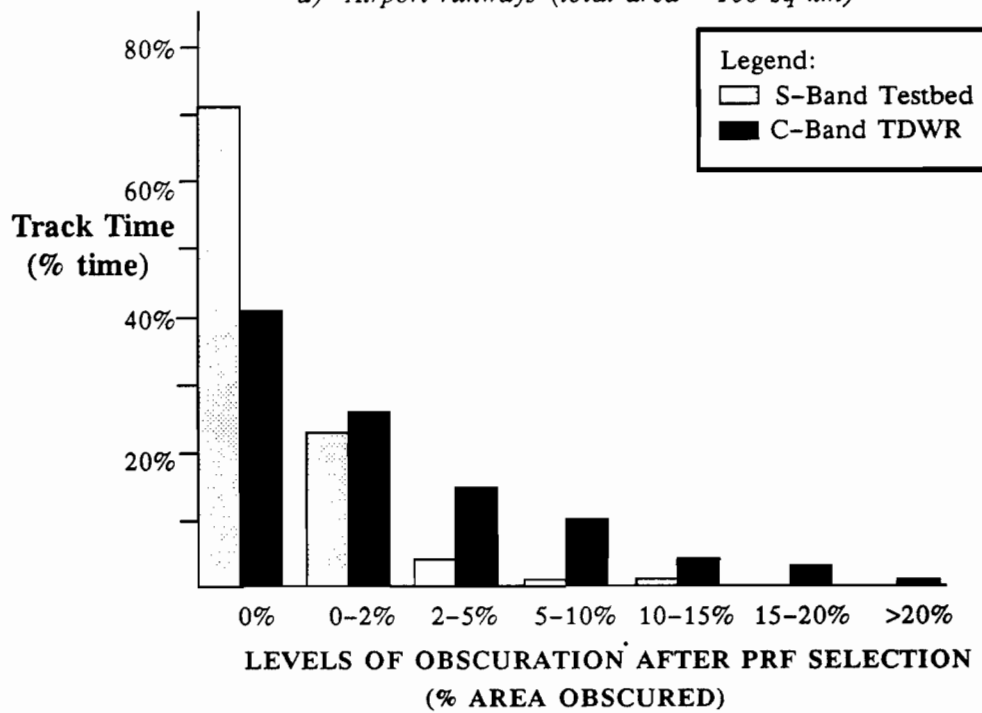a) Airport runways (total area = 100 sq km)
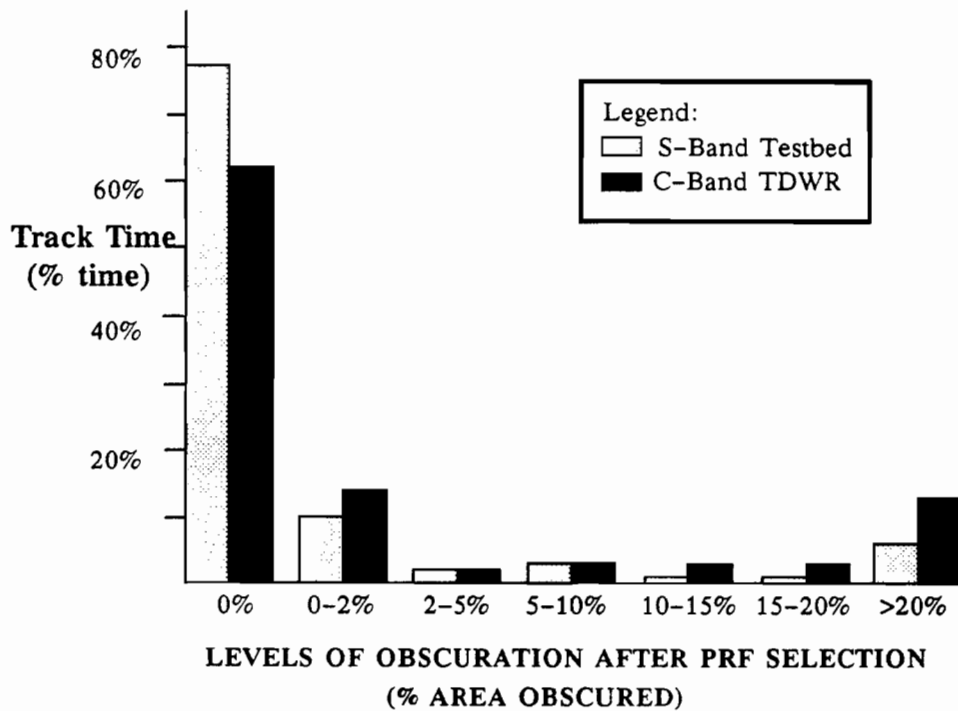
b) 120-deg sector (total area = 1300 sq km)

Figure A-1. Time distribution over total track time of obscuration conditions within Sector 2 micro-burst surveillance region. These represent conditions following adaptive PRF selection for runways and 120-deg sector.
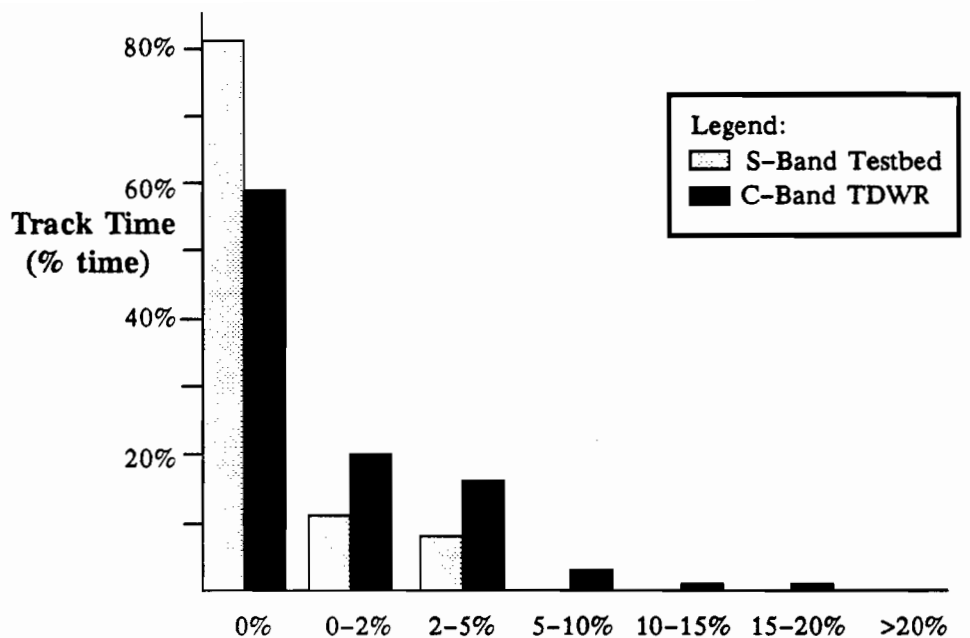
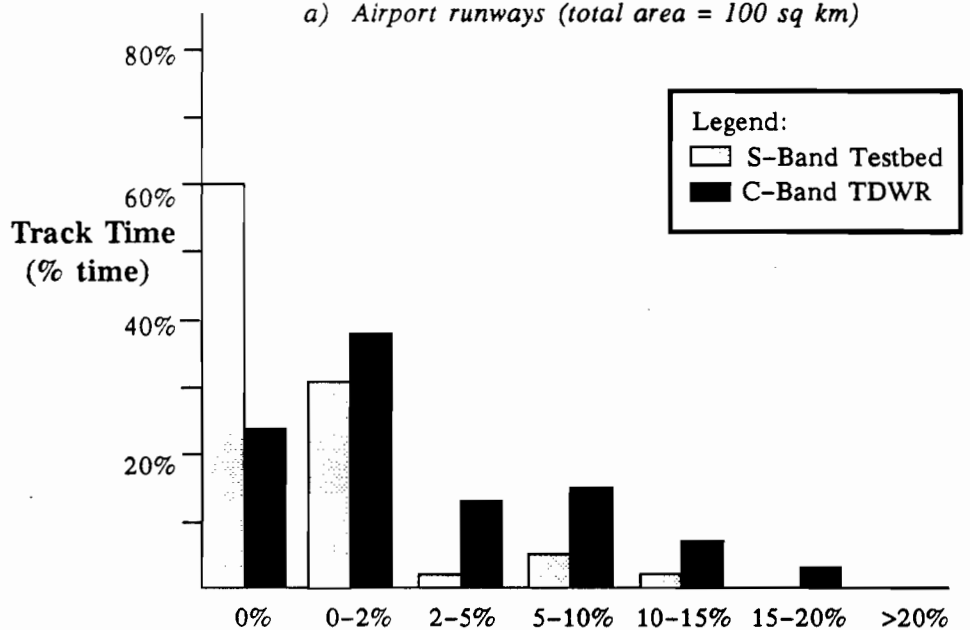*a) Airport runways (total area = 100 sq km)*

b) 120-deg sector (total area = 1300 sq km)

Figure A-2. Time distribution over total track time of obscuration conditions within Sector 3 micro-burst surveillance region. These represent conditions following adaptive PRF selection for runways and 120-deg sector.

a) Airport runways (total area = 100 sq km)

b) 360-deg circle (total area = 11,000 sq km)

Figure A-3. Time distribution over total track time of obscuration conditions within gust front surveillance region. These represent conditions following adaptive PRF selection for runways and 360-deg circle.